

Evolution of Fermi Liquid Behavior with Doping in the Hubbard Model

Jungsoo Kim and D. Coffey

Department of Physics, State University of New York, Buffalo, NY 14260

(November 12, 2018)

Abstract

We calculate the single-particle Green's function for the tight-binding band structure, $\xi_{\vec{p}} = -2t \cos p_x - 2t \cos p_y - \mu$, with a function of chemical potential μ for square-lattice system. The form of the single-particle self-energy, $\Sigma(\vec{p}, E)$, is determined by the density-density correlation function, $\chi(\vec{q}, \omega)$, which develops two peaks for $\mu \gtrsim -2.5t$ unlike parabolic band case. Near half filling $\chi(\vec{q}, \omega)$ becomes independent of ω , one dimensional behavior, at intermediate values of ω which leads to one dimensional behavior in $\Sigma(\vec{p}, E)$. However $\mu \leq -0.1t$ there is no influence on the Fermi Liquid dependences from SDW instability. The strong \vec{p} and E dependence of the off-shell self-energy, $\Sigma(p, E)$, found earlier for the parabolic band is recovered for $\mu \lesssim -t$ but deviations from this develop for $\mu \gtrsim -0.1t$. The resonance peak width of the spectral function, $A(\vec{p}, E)$ has linear dependence in $\xi_{\vec{p}}$ due to the E dependence of the imaginary part of $\Sigma(\vec{p}, E)$. We point out that an accurate detailed form for $\Sigma(\vec{p}, E)$ would be very difficult to recover from ARPES data for the spectral density.

71.10.-w

I. INTRODUCTION

The Fermi liquid(FL) theory has been used to describe metallic phase in which quasi-particle concept develops from a free electron model to study the metallic behavior [1]. Since the discovery of high temperature superconductivity in the cuprates [2], the normal state properties of the quasi-two dimensional cuprates have been investigated experimentally and theoretically. The experimental observations such as optical conductivity [3], electrical resistivity [4-6] and angle resolved photoemission spectroscopy(ARPES) [7,8] do not follow the conventional FL behaviors. The absence of those FL dependences has lead to a proposal that FL model for these quasi-low dimensional conductors should be discarded in favor of a Luttinger liquid-like model [9] in which there is a separation of charge and spin degrees of freedom in the elementary excitation.

However Castellani, Di Castro and Metzner have shown that the FL regime is recovered for dimensions greater than one, having investigated instability of Luttinger liquid(LL) by analyzing correlated fermions with anisotropic hopping amplitudes in one dimensional system [10] and dimensional crossover FL to LL using analytic continuation for non-integer dimensions [11]. Independent calculations show that arbitrarily small transverse hopping kills off LL [12,13]. They also found no breakdown of the perturbation theory.

Given that the expected FL dependences are based on parabolic band (a spherical Fermi surface model) and a quasi-particle approximation and assuming that the ground state is analytically continuous to the non interacting ground state as a function of interaction strength, the discrepancy between the FL picture and the experiment has two possibilities. Firstly the conventional FL dependences are present but they are limited to anomalously low energy and temperature scales induced by interactions among the fermions or by the band structure of the non-interacting fermions. In this picture the spectral density of the single-particle Green's function is still characterized by a single-particle like sharp resonance for momenta very close to the Fermi surface whose width becomes progressively broader as the quasi-particle momenta move further from the Fermi surface where the quasiparticle approximation breaks down. The second possibility can be viewed as an extreme case of the first possibility in which interactions are so strong that the quasi-particle approximation breaks down over at least some region of the Fermi surface. In this case the ground state is still a FL in that it has developed analytically out of the non-interacting ground state. This picture is supported by ARPES measurements [14,15] on the underdoped cuprates although the quasi-particle peaks remain anomalously broad ever at the chemical potential [16]. In these experiments the Fermi surface seems to develop around a particular direction, signaled by a quasi-particle peak in the measured spectral density at low doping. The region in which there is a Fermi surface defined by the vanishing of a quasi-particle peak grows with doping until the whole surface is established. [8] The absence of a quasiparticle peak is referred to as a pseudogap. Previously this type of data for underdoped cuprates had been described in terms of hole pockets which were shown to arise from strong correlation effects in calculations of the t-J model [17-20]. However a search for these pockets in the recent ARPES results [8] was unsuccessful.

The leading 2D FL behavior for on-shell self-energy with an isotropic band structure at zero temperature, $\xi_{\vec{p}} = \frac{\vec{p}^2}{2m} - \frac{p_f^2}{2m}$, is

$$\Sigma'(\vec{p}, \xi_{\vec{p}}) = -\alpha\xi_{\vec{p}} - \frac{\pi}{2}\beta\xi_{\vec{p}}|\xi_{\vec{p}}| - \gamma|\xi_{\vec{p}}|^{5/2} + O(\xi_{\vec{p}}^3) \quad (1a)$$

$$\Sigma''(\vec{p}, \xi_{\vec{p}}) = \beta\xi_{\vec{p}}^2 \ln |\xi_{\vec{p}}/\xi_0| + O(\xi_{\vec{p}}^4) \quad (1b)$$

where the cut-off energy ξ_0 is isotropic [21]. These leading on-shell dependences of imaginary part of self-energy had been determined previously by a number of authors [22,23]. For low-density system ξ_0 goes to zero so that the region of the generic Fermi liquid behavior is limited. The $\xi_{\vec{p}}|\xi_{\vec{p}}|$ energy dependence in the real part is a mirror of the imaginary part of the self-energy, $\beta\xi_{\vec{p}}^2 \ln \xi_{\vec{p}}$, through Kramers-Kronig relation which gives a T^2 contribution to the specific heat in addition to that from zero sound [24]. The $|\xi_{\vec{p}}|^{5/2}$ term is the leading zero-sound contribution. This term has a corresponding $(\xi_{\vec{p}} - \xi_{th})^{3/2}$ term in $\Sigma''(\vec{p}, \xi_{\vec{p}})$, where $\xi_{th} = (v_{zs} - v_f)p_f$, determined by the velocity of the zero-sound mode. 2D calculation shows no evidence of a breakdown in FL theory and is similar to 3D FL considering a parabolic band. The cut-off energy, ξ_0 , has a corresponding cut-off temperature, T_0 , which restricts the leading correction to FL behavior in $\Sigma''(p, \xi_p, T)$ so that T behavior will take over the FL behavior at low density limit [21]. These cut-offs are determined by quasiparticle interactions and the characteristic energy of the non-interacting system, E_f . As the system goes to quasi 1D band which can be modeled by considering different ratio of t_x and t_y , for example quasi 1D organic materials such as $(TMTSF)_2X$ or $BEDT - TTF$ [25], van Hove singularity moves to the bottom of the band so that particle-hole(ph) pair contribution is more important than particle-particle(pp) contribution for low density limit. In this case the nature of the q1D FL behavior remains similar to that of 2D FL [26]. For parabolic band structure pp channel which leads Cooper instability is more important than ph channel in 3D and vice versa in 1D due to the density of states. No particular set of diagrams is significant in 2D [27], but at least the second order calculation is shared by both of them so that functional dependence in either one will represent the FL behavior. The pp channel is discussed later in this paper.

The cuprates have an anisotropic band-structure which can lead to strong band structure features in the density of states. This anisotropy of the band structure is used in a number of different models to explain the lack of FL dependences in experiment [28,29]. The anisotropy has been invoked to describe transport data in the hot spot [30] and cold spot [31] models. In the hot spot model it is proximity to the SDW instability that is important whereas in the cold spot model it is proximity to the superconducting phase through pairing fluctuations which leads to the anisotropy. More recently renormalization group calculation have shown that if the Fermi surface is dominated by a set of saddle points in the density of states Landau FL theory, the quasi-particle approximation to FL theory, can breakdown [32,33].

The Hubbard model has been employed extensively in theoretical investigations of the normal state properties of the cuprates because the tight binding band structure and short-range Coulomb correlations result in an effective magnetic Hamiltonian for low doping which is consistent with the data. We investigate the FL characteristics of this model as a function of chemical potential, μ , from $\mu = -3t$ where the Fermi surface is a circle to $\mu = -0.1t$, near half-filling, where it is almost a square. A 2D nearest neighbor tight-binding band structure, $\xi_{\vec{p}} = -2t \cos p_x - 2t \cos p_y - \mu$, will be used to determine the momentum and energy dependence of single properties in FL behavior where t is the nearest neighbor hopping constant. Near the half-filling curved \bar{M} points are connected by flat Fermi surface which is

a good model for the band structure of BSCCO in which there is a strongly nested vector [34]. The Hamiltonian includes a repulsive contact interaction which we treat in the weak coupling approximation. By introducing a cut-off, q_c , for the interaction in momentum space the influence of long wavelength interactions on $\Sigma(\vec{p}, E)$ in the ph channel has been investigated in this model and shown to determine the functional form of $\Sigma(\vec{p}, E)$ at low energies as in the parabolic band case. The evolution of the leading behaviors in real and imaginary part is determined by the changes in the bare ph propagator as the Fermi surface becomes more anisotropic. First we calculate the contribution to $\Sigma(\vec{p}, \xi_{\vec{p}})$, the on-shell self-energy, to the second order in V which gives the functional form of the corrections and then consider the effect of the repeated scattering from ph channel which would indicate the influence of any instabilities in these behaviors.

We next calculate the off-shell self-energy, $\Sigma(\vec{p}, E)$, which is probed directly in angle resolved photoemission through the spectral density $A(\vec{p}, E)$. It is found that energy dependence of the imaginary part of $\Sigma(\vec{p}, E)$ leads to a width of the quasi-particle resonance in $A(\vec{p}, E)$ which is linear in $\xi_{\vec{p}}$ even when the on-shell $\Sigma''(\vec{p}, E)$ has the expected $\xi_{\vec{p}}^2 \ln \xi_{\vec{p}}$ dependence. We point to the difficulty of extracting the functional form of off-shell self-energy from ARPES data on the spectral function.

II. CALCULATIONS

From the Hamiltonian

$$H = \sum_{\vec{p}, \sigma} \xi_{\vec{p}} c_{\vec{p}, \sigma}^\dagger c_{\vec{p}, \sigma} + \sum_{\vec{p}, \vec{q}, \sigma, \sigma'} V(\vec{q}) c_{\vec{p}, \sigma}^\dagger c_{\vec{p}', \sigma'} c_{\vec{p}' - \vec{q}, \sigma'}^\dagger c_{\vec{p} + \vec{q}, \sigma} \quad (2)$$

where $\xi_{\vec{p}}$ is the electronic band structure and V is the electron-electron interaction which is treated as a perturbation term, the single-particle self-energy, $\Sigma(\vec{p}, E) = \Sigma'(\vec{p}, E) + i\Sigma''(\vec{p}, E)$, is given by

$$\Sigma(\vec{p}, iE_n) = -T \sum_{\vec{q}, \omega_l} G(\vec{p} - \vec{q}, iE_n - \omega_l) V_{eff}(\vec{q}, \omega_l) \quad (3)$$

where $G(\vec{p}, iE_n)$ is the unperturbed temperature Green's function and ω_l is Bose Matsubara frequencies. The V_{eff} includes all the ph diagrams in principle. As a function of filling the electronic band structure develops an anisotropic Fermi surface which will end up with quasi-one dimensional square Fermi surface at $\mu = 0$. As the system goes to half-filling, the density of states at the Fermi surface approaches to the Van Hove singularity, which makes ph channel more significant in the low filling system. We are to concentrate on two directions in momentum space through out the calculations, $(1, 0)p$ and $(1, 1)p$, which are extreme directions in the tight-binding band structure.

The accurate calculation of the density-density correlation function is essential in this study. The correlation function, $\chi(\vec{q}, \omega) = \chi'(\vec{q}, \omega) + i\chi''(\vec{q}, \omega)$, for ph channel is given by

$$\chi(\vec{q}, \omega) = \sum_{\vec{p}} \frac{f(\xi_{\vec{p} + \vec{q}}) - f(\xi_{\vec{p}})}{\omega - (\xi_{\vec{p} + \vec{q}} - \xi_{\vec{p}})} \quad (4)$$

where $\xi_{\vec{p}} = -2t \cos p_x - 2t \cos p_y - \mu$. The imaginary part of the density-density correlation function for the tight-binding band structure is given by

$$\chi''(\vec{q}, \omega > 0) = \frac{1}{4\pi} \int dp_x \int dp_y \frac{\Theta(\xi_{\vec{p}})\Theta(-\xi_{\vec{p}-\vec{q}})\delta(p_y - p_y^*)}{|-4t\sqrt{\sin^2 \frac{q_y}{2} - [\frac{\omega}{4t} - \sin(p_x - \frac{q_x}{2}) \sin \frac{q_x}{2}]^2}|} \quad (5a)$$

$$p_y^* = \sin^{-1}\left[\frac{\omega - 4t \sin(p_x - \frac{q_x}{2}) \sin \frac{q_x}{2}}{4t \sin \frac{q_x}{2}}\right] + \frac{q_y}{2} \quad (5b)$$

in which subscripts, x and y , can be switched when $q_y < q_x$. The Kramers-Kronig relationship is used to calculate the real part of the correlation function. The $(1, 0)q$ or $(0, 1)q$ direction can be handled by the expression,

$$\chi''_{10q}(\omega) = \frac{1}{2\pi} \frac{p_f(p_1)\Theta(p_{f,max}^2 - p_1^2) - p_f(p_2)\Theta(p_{f,max}^2 - p_2^2)}{\sqrt{(4t \sin \frac{q}{2})^2 - \omega^2}} \Theta\left[1 - \left(\frac{\omega}{4t \sin \frac{q}{2}}\right)^2\right] \quad (6)$$

where $p_f(p) = \cos^{-1}[-\frac{\mu}{2t} - \cos(p)]$, $p_{f,max} = \cos^{-1}[-1 - \frac{\mu}{2t}]$, $p_1 = \sin^{-1}[\frac{\omega}{4t \sin(q/2)}] - \frac{q}{2}$ and $p_2 = \sin^{-1}[\frac{\omega}{4t \sin(q/2)}] + \frac{q}{2}$. Unlike the parabolic band structure the anisotropy of the system in the tight-binding band structure restricts the solution of the delta function to different areas of the Fermi surface as the chemical potential approaches to half-filling and a direction of the system aligns $(1, 1)q$. For a given ω , the solutions of the delta function come from two different regions of Fermi surface. Only one of these contribute for the $\vec{q} = (1, 0)q$ direction, whereas both of them survive in $\vec{q} = (1, 1)q$ direction in the long wavelength limit.

On the ph channel the short wavelengths do not affect the logarithmic behavior in $\Sigma''(\vec{p}, \xi_{\vec{p}})$ but do contribute to the cut-off energy, ξ_0 . At half-filling with $q = 2p_f$, the correlation function diverges in both real and imaginary part which will reflect SDW instability [35,36]. Hence by restricting a range of the interaction we tune the cut-off momentum, q_c , in the self-energy calculation to identify the values of q which are responsible for FL energy dependence.

First we discuss results of the 2nd order calculation in the next section which will show the FL energy dependences in the function of band structure and we evaluate and discuss the repeated scattering case and Stoner instability. Except in $\mu \rightarrow 0$ limit, there is no nesting phenomena from short wave length which solely contribute the cut off energy, ξ_0 without affecting the log behavior. We consider two different regions of μ separately as in anisotropic 2D FL and quasi 1D FL.

A. 2nd order calculation of $\Sigma(\vec{p}, \xi_{\vec{p}})$

The self-energy at zero temperature for second order calculation is given by

$$\Sigma(\vec{p}, E > 0) = \sum_{\vec{q}} \Theta(E - \xi_{\vec{p}-\vec{q}})\Theta(\xi_{\vec{p}-\vec{q}})V_{\vec{q}}^2 \chi(\vec{q}, E - \xi_{\vec{p}-\vec{q}}) \quad (7)$$

where $\chi(\vec{q}, \omega)$ is the density-density correlation function or response function and $V_{\vec{q}} = V\Theta(q_c - |\vec{q}|)$ in which $q_c = \pi$ and $V = t$ throughout the calculations. The $\xi_{\vec{p}}^2 \ln \xi_{\vec{p}}$ behavior in the imaginary part of the self-energy comes from the linear energy dependence in $\chi''(\vec{q}, \omega)$. In the self-energy calculation the energy dependence is mainly determined by the frequency dependence of the density-density correlation function rather than the step functions in the expression for the self-energy. Since the second order contribution is common for both of ph and pp channel, the second order calculation reveals the functional dependence of FL behavior as a function of chemical potential which we break in two regions, 2D and quasi-1D.

1. Anisotropic 2D Fermi Liquid : $-4t \leq \mu \leq -t$

As the chemical potential, μ , goes to zero, flatness of Fermi surface along $(1, 1)p$ direction develops. Although the Fermi surface develops flat, quasi-one dimensional, regions for $\mu \sim -t$, no signature of quasi-one dimensional behavior is seen in $\Sigma(\vec{p}, E)$. The figure 2 shows the evolution of the response function with a function of μ in the directions of $(1, 0)q$, $(1, 2)q$ and $(1, 1)q$ with $q = 10^{-2}\pi$. The cut-off energies, ω_1^* and ω_2^* , associated with the contributions given momentum \vec{q} are from the two different Fermi surface contributions through the delta function for a given momentum \vec{q} . Those contributions give two different locations of the divergent peaks, ω_1^* and ω_2^* . As \vec{q} points in the $(1, 1)$ direction, ω_1^* approaches zero frequency so that the FL linear behavior is limited to small energies. However even in $(1, 1)q$ direction, the linear piece survives and $\Sigma(\vec{p}, E)$ has FL behavior for $\mu = -t$. As ω_1^* goes to zero energy, the linear behavior in $\chi''(\vec{q}, \omega)$ is limited to a small ω region above which $\chi''(\vec{q}, \omega)$ is independent of ω as $\mu \rightarrow 0$ as in one dimensional system. This will be discussed later. Figure 2 shows the anisotropic band structure effects, ω_1^* and ω_2^* feature, in particle-hole correlation function which first appear around $\mu = 2.5t$. Except $\mu \sim 0$ case, the $\chi''(\vec{q}, \omega)$ follows $\omega/|\vec{q}|$ at small ω which leads to $\xi_{\vec{p}}^2 \ln \xi_{\vec{p}}$ form for $\Sigma''(\vec{p}, \xi_{\vec{p}})$.

The log behavior of the imaginary part of the on-shell self-energy comes from long wave length calculation. The figure 3 demonstrates contributions $|\vec{q}| \leq \frac{\pi}{10}$ in $\chi(\vec{q}, \omega)$ to the imaginary part of on-shell self-energy with six different sets of $|\vec{q}|$ values given by $10^{-n}\pi \leq |\vec{q}| \leq 10^{-(n-1)}\pi$ where $n = 6, 5, 4, 3, 2, 1$. For small values of $|\xi_{\vec{p}}/t|$ the contributions from longer wavelengths provide the $\xi_{\vec{p}}^2 \ln \xi_{\vec{p}}$ dependences whereas shorter wavelengths lead to contributions to the $\xi_{\vec{p}}^2$ dependence. The log behavior is restricted by small energy and the $|\vec{q}|$ s which are long wavelength. The anisotropic 2D systems with $-4t \leq \mu \leq -t$ shows generic FL behavior with increasing anisotropy in \vec{p} . The correction term is enhanced by tuning the chemical potential close to zero and will be discussed in the next section. The cut-off, ξ_0 , and β for the two directions of \vec{p} reflect the growing anisotropy of the Fermi surface as μ changes from $-3t$ to $-t$.

2. Quasi-1D behavior : $-t \leq \mu \leq 0$

The purely one dimensional response function with a tight-binding band structure, $\xi_p = -2t \cos p - \mu$, is

$$\chi''_{1D}(q, \omega) = \frac{1}{2} \frac{\Theta(p_f - |\frac{q}{2} - \sin^{-1}(\frac{\omega}{4t \sin \frac{q}{2}})|) - \Theta(p_f - |\frac{q}{2} + \sin^{-1}(\frac{\omega}{4t \sin \frac{q}{2}})|)}{|4t \sin \frac{q}{2} \sqrt{1 - (\frac{\omega}{4t \sin \frac{q}{2}})^2}|} \Theta(1 - |\frac{\omega}{4t \sin \frac{q}{2}}|^2) \quad (8)$$

where $p_f = \cos^{-1}(-\mu/2t)$ is the Fermi level for one dimensional system. In the small frequency limit there is no energy dependence in χ''_{1D} which has corresponding logarithmic divergence in χ'_{1D} ,

$$\chi'_{1D}(q, \omega = 0) = \frac{1}{-4t\pi \sin(q/2)} \ln \left| \frac{\tan(p_f - q/2)}{\tan(p_f + q/2)} \right|. \quad (9)$$

At static limit this divergence at $q = 2p_f$, so called perfect nesting vector, drives the Peierls instability via Kohn anomaly which leads to the metal-insulator transition [37].

Coming back to 2D problem, at $\mu = 0$ the system is one dimensional in that there is perfect nesting between parts on the Fermi surface along $(1, 1)\vec{p}$ direction. Nesting vector, $\vec{q} = (1, 1)\pi$, gives a form

$$\chi''(\pi, \pi, \omega; \mu = 0) = \frac{\pi}{2} \text{sign}(\omega) N(\omega/2) \quad (10)$$

where $N(\omega)$ is density of state which has logarithmic divergence at $\omega = 0$, which breaks quasi-particle picture. For $\mu = 0$ the constant energy dependence at long wavelengths in $\chi''(\vec{q}, \omega)$ which is one dimensional effect lasts up to zero energy. Using the Kramers-Kronig relationship this energy dependence for small $|\vec{q}|$ in $\chi''(\vec{q}, \omega)$ leads to a $\ln \omega$ divergences in the real part, $\chi'(\vec{q}, \omega)$, signaling the break down of RPA. The large $|\vec{q}|$ behavior is shown in figure 5 where it is clear that the $\ln \omega$ divergence in $\chi''(\vec{q}, \omega)$ is rapidly destroyed as μ goes away from half-filling.

For $|\vec{q}| < 10^{-1}\pi$ structure of χ'' , two divergent peaks identified by ω_1^* and ω_2^* , follows the discussion in previous section. Due to rapid development of frequency independence in χ'' for low energies as $\mu \rightarrow 0$, the quasi 1D corrections to $\xi_{\vec{p}}^2 \ln \xi_{\vec{p}}$ behavior of $\Sigma''(\vec{p}, \xi_{\vec{p}})$ at intermediate values of ω have a $\xi_{\vec{p}}^{3/2}$ dependence in the quasi-particle life time. This is shown in figure 7 for $\mu = -0.1t$ in which the Fermi surface is flat over an extended area. The $\xi_{\vec{p}}^{3/2}$ correction sets in at $\xi_{\vec{p}} \sim 0.02t$, which limits generic FL behavior to small region. As μ goes away from half filling, the logarithmic divergence in ω dies out rapidly as in the figure 5 so that the system is far from a Peierls-like instability. The second order calculation shows that quasi-particle life time has generic FL dependence with $\mu \neq 0$ with a $\xi_{\vec{p}}^{3/2}$ term as a correction to $\xi_{\vec{p}}^2 \ln \xi_{\vec{p}}$ when $\mu \lesssim 0$.

B. RPA calculation of $\Sigma(\vec{p}, \xi_{\vec{p}})$

1. Long wavelength contribution

With $\mu \neq 0$ the long wavelength limit contribution which is responsible for $\xi_{\vec{p}}^2 \ln \xi_{\vec{p}}$ or $\xi_{\vec{p}}^{3/2}$ for $\mu \sim 0$ survives unless the strong interaction limit is considered in RPA. The effective interaction in equation (2) for repeated scattering involves in two independent channels, the symmetric and the antisymmetric channels, followed by spin exchanges of 0 and 1 and is given by

$$V_{eff}(\vec{q}, \omega) = \frac{1}{2} \frac{V_s^2 \chi(\vec{q}, \omega)}{1 - V_s \chi(\vec{q}, \omega)} + \frac{3}{2} \frac{V_a^2 \chi(\vec{q}, \omega)}{1 - V_a \chi(\vec{q}, \omega)} \quad (11)$$

where $V_s = V_q$ and $V_a = -V_q$. In RPA the imaginary part of self-energy, $\Sigma''(\vec{p}, \xi_{\vec{p}})$, is just enhanced from the second order calculations as in figure 8. $\mu = -0.1t$ case includes $\xi_{\vec{p}}^{3/2}$ corrections in $(1, 0)p$ direction. The real part, $\Sigma'(\vec{p}, \xi_{\vec{p}})$, has $\xi_{\vec{p}} |\xi_{\vec{p}}|$ correction to $\xi_{\vec{p}}$ term. In the figure 9 the $\xi_{\vec{p}}$ term is extracted and comes from long wavelength limit. The $\xi_{\vec{p}} |\xi_{\vec{p}}|$ term is a mirror of $\xi_{\vec{p}}^2 \ln \xi_{\vec{p}}$ term in $\Sigma''(\vec{p}, \xi_{\vec{p}})$ through Kramers-Kronig relationship and the deviations from the fits are consistent to both of $\Sigma''(\vec{p}, \xi_{\vec{p}})$ and $\Sigma'(\vec{p}, \xi_{\vec{p}})$ graphs. The on-shell

calculation of $\xi_{\vec{p}}|\xi_{\vec{p}}|$ term in (1,0) direction with $\mu = -0.1t$ stops at $\xi_{\vec{p}} \sim 0.05t$ because the phase space runs out for that direction and the correction to the $\xi_{\vec{p}}|\xi_{\vec{p}}|$ term sets in earlier than (1,1) direction. The coefficients of the $\xi_{\vec{p}}|\xi_{\vec{p}}|$ terms for the two directions are different due to anisotropy of the system.

The figure 10 shows the functional dependence of the cut-off energy in imaginary part of the self-energy, $\xi_{0,\vec{p}}$, and the coefficients, $\beta_{\vec{p}}$, for the tight-binding band structure. The anisotropy from $\beta_{\vec{p}}$ grows as the band is filled, but near half filling the trend changes rapidly due to the flatness of the band structure. The cut-off energy shows anisotropy even at $\mu = -3t$ which is different from the figure 2 in which the anisotropic effects of splitting the two different peaks in $\chi''(\vec{q},\omega)$.

2. Instabilities

As discussed above the correlation function itself does not indicate any instability unless $\mu = 0$ as in figure 5. For the repulsive interaction antisymmetric channel in effective interaction could have an instability indicated by a pole at $\omega = 0$ in the effective interaction. The solution for it is given by $1/V_{\vec{q}} = \chi'(\vec{q}, \omega = 0)$ in RPA in which there is divergence with perfect nesting vector at $\mu = 0$ so that there are solutions for all $|V_{\vec{q}}|$'s. Within the RPA the question is how fast the system goes to 1D as a band approaches to half-filling.

In parabolic band structure, the real part of the correlation function in static limit is given by

$$\chi_{1D}(q) = N_{1D}(0) \frac{1}{2(q/2p_f)} \ln \left| \frac{1 + (q/2p_f)}{1 - (q/2p_f)} \right| \quad (12a)$$

$$\chi_{2D}(q) = N_{2D}(0) \left[1 - \frac{\sqrt{(q/2p_f)^2 - 1}}{(q/2p_f)} \theta\{(q/2p_f) - 1\} \right] \quad (12b)$$

$$\chi_{3D}(q) = N_{3D}(0) \left[\frac{1}{2} + \frac{1 - (q/2p_f)^2}{4(q/2p_f)} \ln \left| \frac{1 + (q/2p_f)}{1 - (q/2p_f)} \right| \right] \quad (12c)$$

where $N(0)$ s are the densities of state on Fermi level for each dimensions and θ is a step function. In 2D the correlation function has a cusp and a discontinuous derivative at $q = 2p_f$ due to the step function whereas 3D case varies smoothly. Since the Fermi surface consists of two points in 1D, the nesting condition $\xi_{\vec{p}} - \xi_{\vec{p}+2\vec{p}_f}$ is satisfied over the entire Fermi surface resulting in a log divergence at $q = 2p_f$ which is responsible for the breakdown of the quasiparticle picture leading to a metal-insulator transition.

The figure 11 the static correlation function in (1,1) \vec{q} direction has a developing divergence at $|\vec{q}| = 2p_f^{(1,1)}$ as the system changes 2D to 1D. The function is repeated at $|\vec{q}| = \pi$ due to periodic lattice where $|\vec{q}| = \pi$ is at the middle of the dip right next to the peak. $\mu = -3t$ which has the Fermi surface close to circle shows constant q dependence with densities of state

$$N(\mu) = \lim_{\vec{q} \rightarrow 0} \lim_{\omega \rightarrow 0} \chi'(\vec{q}, \omega) \quad (13)$$

as in parabolic band case. The phase diagram, $V_{\vec{q}}$ vs. μ , is calculated by $1/V_{\vec{q}} = \chi'(2p_f, 2p_f, \omega = 0)$. With a interaction strength of $V_q = t$, the Stoner instability does not occur until $\mu \sim -0.03t$. In the calculations discussed in this paper $V_q = t$ dotted line in figure 12 so that the instability of the system is absent except when $\mu \sim 0$ for $V_q \leq t$.

This conclusion is supported by a recent renormalization group analysis of the Hubbard model by Halboth and Metzner [38] who found that the tendency towards the antiferromagnetic nesting instability is limited to $\mu \lesssim -0.1t$ for $U = t$ as evidenced by a growing spin susceptibility. They found in fact that $d_{x^2-y^2}$ superconductivity fluctuations provide the dominant susceptibility further from half filling but even these were suppressed beyond $\mu \sim -0.01t$. The influence of superconducting fluctuations are missing in the present calculation [39].

Going beyond this weak-coupling region is difficult because of the uncontrolled nature of the RPA. One such attempt is the so-called self-consistent fluctuation exchange approximation (FLEX) which however is equally uncontrolled. It has been pointed out by Trembley and coworkers that the absence of vertex corrections in the FLEX leads even more severe breakdowns of sum rules than does the RPA discussed here. Vilk and Trembley have proposed an improvement in RPA to ensure that the sum rules are satisfied. In the approach the influence of the cross channels in the ph expansion on the vertices is mimicked by letting the irreducible vertices in the charge and spin channels be independent of each and chosen to satisfy sum rules. In this approach SDW fluctuations above $T = 0$ lead to the breakdown of the quasi-particle approximation for $U = 4t$. These approaches have been limited to finite size systems and so miss the long wavelength interactions responsible for the leading corrections of interest in the present work.

3. Contributions from the Particle-Particle Channel

Fukuyama et al. [40] have investigated the contribution to $\Sigma''(\vec{p}, E)$ for the pp channel using the parabolic dispersion. The contribution to $\Sigma(\vec{p}, E)$ in second order in the interaction can be thought of as being in either the ph or pp channel. In the second order calculation the difference between the two channels is that $\xi_p^2 \ln \xi_{\vec{p}}$ contribution comes from propagating particle or hole pairs with momenta $q \sim 2p_f$ in pp channel whereas it comes from long-wavelength particle-hole pairs in ph channel as we shown above in figure 3. Taking the second order diagram to be in the pp channel contribution, its contribution is screened by repeated scattering in that channel. In contrast to the case of an attractive interaction there is no Cooper instability but instead the contribution is reduced by the repeated scattering. Unlike the situation in the ph channel the result is not simply an enhancement or reduction of the contribution from the second order diagram giving $\xi_p^2 \ln \xi_p$ contribution to $\Sigma''(p, \xi_p)$ again. Rather there is a strong momentum dependence in real part of the pp propagator at $q \sim 2p_f$ which eliminates the $\xi_p^2 \ln \xi_p$ dependence. As a result the effect of including the pp channel in a calculation of $\Sigma(p, E)$ is to remove the contribution of the second order term in the interaction from leading dependences. The pp contribution to $\Sigma(p, E)$ in a tight binding bandstructure remains to be worked out in detail. However the result is unlikely to be quantitatively different from the result for the parabolic band. Indeed for particle-pairs/hole-pairs with net momentum $\vec{Q} = (\pi, \pi)$ it is easy to show that the propagator $K(\vec{Q}, \omega)$ behaviors as $K(\vec{Q}, \omega) \sim \frac{1}{\omega+2\mu} f(\mu)$ where $f(\mu)$ is a polynomials in μ and gives a

vanishingly small contribution to $\Sigma(p, E)$ where the consequences of the almost nested Fermi surface would be expected to be greatest.

There have been a number of investigations of collective modes in the pp channel. Engelbrecht and Randeria [41] found a collective mode below the two particle continuum in a bound state of hole pairs which arises because of the finite density of states at bottom of the band in 2D. The contribution of this mode to the self-energy is given by $\Sigma''(p_f, E) \sim \mu |\frac{E}{E_a}|^{5/2}$ where μ is the chemical potential and E_a is an energy scale describing the interaction. So this mode does not contribute to the leading dependences in $\Sigma''(p, E)$. Yang [42] and more recently Demler and Zheng [43] have found evidence for a different singlet and triplet collective mode in the pp channel which exists in a narrow region of momenta near (π, π) . The narrow range of momenta suggests that this mode can have little effect on the low energy properties of $\Sigma(p, E)$.

In summary neither the continuum nor collective mode contributions from the pp channel contribute to the leading dependences in $\Sigma(p, E)$.

C. Off-Shell Calculations, $\Sigma(\vec{p}, E)$: Spectral Function

The spectral function can be measured by ARPES and is given by

$$A(\vec{p}, E) = \frac{|\Sigma''(\vec{p}, E)|}{[E - \xi_{\vec{p}} - \Sigma'(\vec{p}, E)]^2 + [\Sigma''(\vec{p}, E)]^2} \quad (14)$$

where the off-shell self-energies are involved. For large cut-off momentum, q_c , and parabolic band structure the leading contributions to the imaginary part of off-shell self-energy which determines the width of the spectral function has a form [24]

$$\Sigma''(\vec{p}, E) = C[\{\xi_{\vec{p}}^2 + 2\xi_{\vec{p}}(E - \xi_{\vec{p}})\} \ln(\max[\xi_{\vec{p}}, |E|]) + (E - \xi_{\vec{p}})^2 \ln(|E - \xi_{\vec{p}}|)] \quad (15)$$

where C is a constant. In the figure 13 $[\Sigma''(\vec{p}, E) - \Sigma''(\xi_{\vec{p}}, \vec{p})]/(E - \xi_{\vec{p}})$ vs. $\ln |E - \xi_{\vec{p}}|$ is plotted for $E - \xi_{\vec{p}} < 0$. In the limit $(E - \xi_{\vec{p}}) \rightarrow 0$ we find $2C\xi_{\vec{p}} \ln |\xi_{\vec{p}}|$ consistent with equation (15) for given \vec{p} . For $\mu = -2t$ the Fermi surface is close to parabolic band structure and the off-shell self-energy has a $(E - \xi_{\vec{p}})$ independent behavior for small values of $(E - \xi_{\vec{p}})$ as in the equation (15). For $\mu = -0.1t$ the $\Sigma''(p_f, E)$ is consistent with the equation (15). However for $p = 0.95p_f$ although $\Sigma''(\vec{p}, \xi_{\vec{p}})$ still has the $\xi_{\vec{p}}^2 \ln \xi_{\vec{p}}$ dependence, $\Sigma''(\vec{p}, E)$ is seen to deviate from the form given in equation (15). The dependence on E in figure 14 shows a $E^2 \ln |E|$ behavior for $\mu = -2t$ only for $p = p_f$ and the more complicated dependence shown in equation (15) is found for $|\vec{p}| \neq p_f$. This is the case for other values of μ also. This indicates that the form $E^2 \ln E$ for $\Sigma(\vec{p}, E)$ frequently used in the literature is a poor approximation [44,45] to the more complicated function of \vec{p} and E .

ARPES data is analyzed in terms of the single-particle spectral density. The extent to which a quasi-particle resonance is well defined is characterized by the width of the resonance at half-maximum. This is frequently thought of as a measure of the quasi-particle life-time where momentum dependence is taken as a test of the Fermi liquid character of the material under investigation. When the quasi-particle approximation is applied, the spectral function is

$$A(\vec{p}, E) = \frac{\Gamma_{\vec{p}}}{(E - E_{\vec{p}})^2 + \Gamma_{\vec{p}}^2} \quad (16)$$

where $E_{\vec{p}}$ is the location of the resonance and $\Gamma_{\vec{p}}$ is half-maximum width of the peak. Here we apply this analysis to the Hubbard model.

The spectral functions are calculated for $\mu = -2t$ and $\mu = -0.1t$ cases and the widths of the resonance at the half of the peak, $\Gamma_{\vec{p}}$, are plotted as a function of $\xi_{\vec{p}} < 0$. The spectral functions are picked along Γ to Y point and to \bar{M} point. The quasi-particle peaks are well defined and as $p \rightarrow p_f$ resonance gets sharper for $(1, 0)p$ and $(1, 1)p$ directions in the figure 15 for $\mu = -2t$. The $\mu = -0.1t$ case in the figure 16 has the same feature except growing anisotropic feature for $(1, 1)p$ direction in deep inside of the Fermi surface. There is no sign for the pseudogap with the parameters used in this calculations for $\mu = -2t$ and $\mu = -0.1t$. As $p \rightarrow p_f$ the resonance peak does not show symmetry about $E = E_{\vec{p}}$ since the imaginary part of self energy is always zero for $E = 0$. $A(\vec{p}, E)$ is only symmetric about $E = 0$ for $|\vec{p}| = |p_f|$. The smallest deviation from p_f leads to strongly non-symmetric $A(\vec{p}, E)$. This indicates that one can be misled by assuming symmetry for the ARPES data cutoff by Fermi Dirac distribution function [46] to get the single-particle properties near Fermi surface.

If we expand $A(\vec{p}, E)$ near $E_{\vec{p}} = \xi_{\vec{p}} + \Sigma'(\vec{p}, E)$ which is approximately the location of the resonance peak since $\Sigma(\vec{p}, E)$ is continuous, the width of half maximum is given by the on-shell self-energy

$$\Gamma_{\vec{p}} \sim \frac{z_{\vec{p}} \Sigma''(\vec{p}, E_{\vec{p}})}{\sqrt{1 + [z_{\vec{p}} \partial \Sigma''(\vec{p}, E) / \partial E |_{E=E_{\vec{p}}}]^2}} \quad (17)$$

where $z_{\vec{p}} = [1 - \partial \Sigma'(\vec{p}, E) / \partial E |_{E=E_{\vec{p}}}]^{-1}$ unless $\Sigma''(\vec{p}, E)$ has a strong energy dependences. In this calculation we find $1 - z_{\vec{p}} \lesssim 3\%$ showing that there is very little frequency dependence in the real part, $\Sigma'(\vec{p}, E) \sim \Sigma'(\vec{p}, \xi_{\vec{p}})$. The figure 17 shows the agreement between the half maximum width and the on-shell self-energy at low energies, $\Gamma_{\vec{p}} \sim \Sigma''(\vec{p}, \xi_{\vec{p}})$, for $\mu = -2t$ and $\mu = -0.1t$. As in the figure the generic FL logarithmic behavior is restricted to low energies. For $\mu = -2t$ case $\Gamma_{\vec{p}}$ shows linear behavior in $\xi_{\vec{p}}$ at higher energies which is not extrapolated to zero energy. Clearly the assumption that a deviation from $\Gamma_{\vec{p}} \sim \xi_{\vec{p}}^2 \ln \xi_{\vec{p}}$ or $\xi_{\vec{p}}^2$ is an indication of non-Fermi liquid is not correct. We note that no sign of the complicated $\xi_{\vec{p}}$ and E dependences of $\Sigma(\vec{p}, E)$, shown in equation (15), comes out of this analysis of ARPES data. It seems to us unlikely that it will be possible to recover these dependences without prior knowledge of the functional form to which to fit the data.

III. CONCLUSION AND SUMMARY

We have demonstrated that anisotropy in band structure does not qualitatively change FL dependencies. We have done that by calculating single-particle properties in the Hubbard model in which the shape of the Fermi surface is changed from a circle to a square as the value of the chemical potential is varied from $\mu = -3t$ to $\mu = -0.1t$. In these calculations we have used a weak coupling approximation in which the magnitude of the interaction, V_q , is far from the values for the SDW instability except for $\mu > -0.5t$. Numerical coefficients in the functional forms of the imaginary part of the self-energy reflect the anisotropy of the

band structure but it is not until the Fermi surface is almost a square that the first sign of quasi-1D behavior, $\xi_{\vec{p}}^{3/2}$, appears. As $\mu \rightarrow 0$ the magnitude of $\Sigma''(\vec{p}, \xi_{\vec{p}})$ increases with increasing anisotropy. Also, in the $\mu \rightarrow 0$ limit, an ω independent region in $\chi''(\vec{q}, \omega)$ grows, which is responsible for $\xi_{\vec{p}}^{3/2}$ behavior in $\Sigma''(\vec{p}, \xi_{\vec{p}})$ in $(1, 0)p$ direction. The $\xi_{\vec{p}}|\xi_{\vec{p}}|$ term is also found in $\Sigma'(\vec{p}, \xi_{\vec{p}})$ as in parabolic band case. The instability of the system is slowly developed as the system goes to 1D except $\mu \sim 0$.

The off-shell self-energy is shown to have a similar \vec{p} and E dependence as in the parabolic band with deviations as the Fermi surface develops flat regions. There is no evidence for the pseudogap phenomenon for the parameters used here, $V = t$ and $\mu < -0.1t$. In this region we confirmed the half maximum width of the resonance peak for spectral function is approximated by on-shell self-energy. Asymmetry in the resonance peak grows for $|\vec{p}| = p_f$ due to $\Sigma''(\vec{p}, E = 0) = 0$ and for deep inside of Fermi surface for $\mu = -0.1t$ and $(1, 1)|\vec{p}|$ direction. In the tight binding band structure quasi-particle picture is well defined for $\mu < -0.1t$ and $|V_{\vec{q}}| \lesssim t$.

As one goes further away from this parameter region it becomes difficult to justify the simple RPA weak-coupling approximation used here. SDW and superconducting fluctuations are likely to play a role as other authors have pointed out. Their effects on the leading dependences from long wavelengths in $\Sigma(\vec{p}, E)$ remain to be investigated.

REFERENCES

- [1] D. Pines and P. Nozieres, *The Theory of Quantum Liquids*, Vol.1. Benjamin, New York (1966).
- [2] J. G. Bednorz and K. A. Müller, *Z. Phy. B* **64**, 189 (1986).
- [3] T. Timusk and R. B. Tanner, in *Infrared Properties of High T_c Superconductors*, Vol.1(*Ed.* D. M. Ginsberg), (World Scientific, Singapore, 1988).
- [4] H. Takagi, B. Batlogg, H. L. Kao, J. Kwo, R. J. Cava, J. J. Krajewski and W. F. Peck, *Phys. Rev. Lett.* **69**, 2975 (1992).
- [5] Y. Ando, G. S. Boebinger, A. Passner, T. Kimura and K. Kishio, *Phys. Rev. Lett.* **75**, 4662 (1995).
- [6] Y. Ando, G. S. Boebinger, A. Passner, N. L. Wang, C. Geibel and F. Steglich, *Phys. Rev. Lett.* **77**, 2065 (1996).
- [7] M. C. Schabel, C. H. Park, A. Matsuura, Z. X. Shen, D. A. Bonn, R. Liang and W. N. Hardy, *Phys. Rev. B.* **57**, 6090 and 6107 (1998).
- [8] M. R. Norman, H. Ding, M. Randeria, J. C. Campuzano, T. Yokoya, T. Takeuchi, T. Takahashi, T. Mochiku, K. Kadowaki, P. Guptasarma and D. G. Hinks, *Nature* **392**, 157 (1998); J. Mesot, A. Kaminski, H. M. Fretwell, M. Randeria, J. C. Campuzano, H. Ding, M. R. Norman, T. Takeuchi, T. Sato, T. Yokoya, T. Takahashi, I. Chong, T. Terashima, M. Takano, T. Mochiku, K. Kadowaki, cond-mat 9910430
- [9] P. W. Anderson, *Phys. Rev. Lett.* **64**, 1839 (1990) and **65**, 2306 (1990).
- [10] C. Castellani, C. Di Castro and W. Metzner, *Phys. Rev. Lett.* **69**, 1703 (1992).
- [11] C. Castellani, C. Di Castro and W. Metzner, *Phys. Rev. Lett.* **72**, 316 (1994).
- [12] D. Boies, C. Bourbonnais and A. -M. S. Tremblay, *Phys. Rev. Lett.* **74**, 968 (1995).
- [13] P. Kopietz, V. Meden and K. Schönhammer, *Phys. Rev. B* **56**, 968 (1995).
- [14] H. Ding, M. R. Norman. T. Yokaya, T. Takeuchi, M. Randeria, J. C. Campuzano, T. Takahashi, T. Mochiku and K. Kadowaki, *Phys. Rev. Lett.* **78**, 2628 (1997).
- [15] A. G. Loeser, Z. -X. Shen, M. C. Schabel, C. Kim, M. Zhang, A. Kapitulnik and P. Fournier, *Phys. Rev. B.* **56**, 14185 (1997).
- [16] J. Mesot, A. Kaminski, H. M. Fretwell, M. Randeria, J. C. Campuzano, H. Ding, M. R. Norman, T. Takeuchi, T. Sato, T. Yokoya, T. Takahashi, I. Chong, T. Terashima, M. Takano, T. Mochiku and K. Kadowaki, cond-mat 9910430.
- [17] S. A. Trugman, *Phys. Rev. Lett.* **65**, 500 (1990).
- [18] A. Moreo, D. J. Scalapino, R. L. Sugar, S. R. White and N. E. Bickers, *Phys. Rev. B* **41**, 2313 (1990).
- [19] R. Eder and Y. Ohta, *Phys. Rev. B* **51**, 6041 (1995).
- [20] E. Dagotto, A. Nazarenko and M. Boninsegni, *Phys. Rev. Lett.* **73**, 728 (1994).
- [21] J. Kim and D. Coffey, *Phys. Rev. B* **57**, 542 (1998).
- [22] C. Hodges, H. Smith and J. W. Wilkins, *Phys. Rev.* **4**, 302 (1971).
- [23] P. Bloom, *Phys. Rev. B* **12**, 125 (1975).
- [24] D. Coffey and K. Bedell, *Phys. Rev. Lett.* **71**, 1043 (1993).
- [25] J. M. Williams *et al.*, *Organic Superconductors (including fullerenes) : synthesis, structure, properties and theory* (Prentice Hall, Englewood Cliffs, 1992).
- [26] J. Kim and D. Coffey, unpublished.
- [27] J. Kim and D. Coffey, *Philos. Mag. B* **74**, 477 (1996).
- [28] A. Virosztek and J. Ruvalds, *Phy. Rev. B* **42**, 4064 (1990).

- [29] J. Ruvalds and A. Virosztek, *Phys. Rev. B* **43**, 5498 (1991).
- [30] R. Hlubina and T. M. Rice, *Phys. Rev. B* **51**, 9253 (1995).
- [31] L. B. Ioffe and A. J. Millis, *Phys. Rev. B* **58**, 11631 (1998).
- [32] N. Furukuyama and T. M. Rice, *J. Phys. C* **10** L381 (1998).
- [33] N. Furukuyama and T. M. Rice, *Phys. Rev. Lett.* **81** 3195 (1998).
- [34] D. S. Dessau, Z. -Z. Shen, D. M. King, D. S. Marshall, L. W. Lombardo, P. H. Dickinson, A. G. Loeser, J. DiCarlo, C. -H. Park, A. Kapitulnik and W. E. Spicer, *Phys. Rev. Lett.* **71**, 2781 (1993).
- [35] J. E. Hirsch and D. J. Scalapino, *Phys. Rev. Lett.* **56**, 2732 (1986).
- [36] P. A. Lee, and N. Read, *Phys. Rev. Lett.* **58**, 2691 (1987).
- [37] M. J. Rice and S. Strässler, *Solid State Commun.* **13**, 125 (1973).
- [38] C. J. Halboth and W. Metzner, cond-mat 9908471.
- [39] D. Zanchi and H. J. Schulz, *Eur. Phys. Lett.* **44** 235 (1998); cond-mat 9812303.
- [40] H. Fukuyama and Y. Hasegawa, *Prog. Theor. Phys Suppl.* **101** 441 (1990); H. Fukuyama, Y. Hasegawa and O. Narikiyo, *J. of Phys. Soc. Jpn.* **60**, 2013 (1991).
- [41] J. R. Engelbrecht and M. Randeria, *Phys. Rev. Lett.* **65** 1032 (1990); *Phys. Rev. B* **45** 12419 (1992).
- [42] C. N. Yang, *Phys. Rev. Lett.* **63**, 2144 (1989).
- [43] E. Demler and S-C. Zheng, *Phys. Rev. Lett.* **75**, 4126 (1995).
- [44] G. Jackeli and V. Y. Yushankhai, *Phys. Rev. B* **56**, 3540 (1997).
- [45] D. Menashe and B. Laikhtman, *Phys. Rev. B* **59** (1999).
- [46] M. R. Norman, H. Ding, H. Fretwell, M. Randeria and J. C. Campuzano, *Phys. Rev. B* **60**, 7585 (1999).

FIGURES

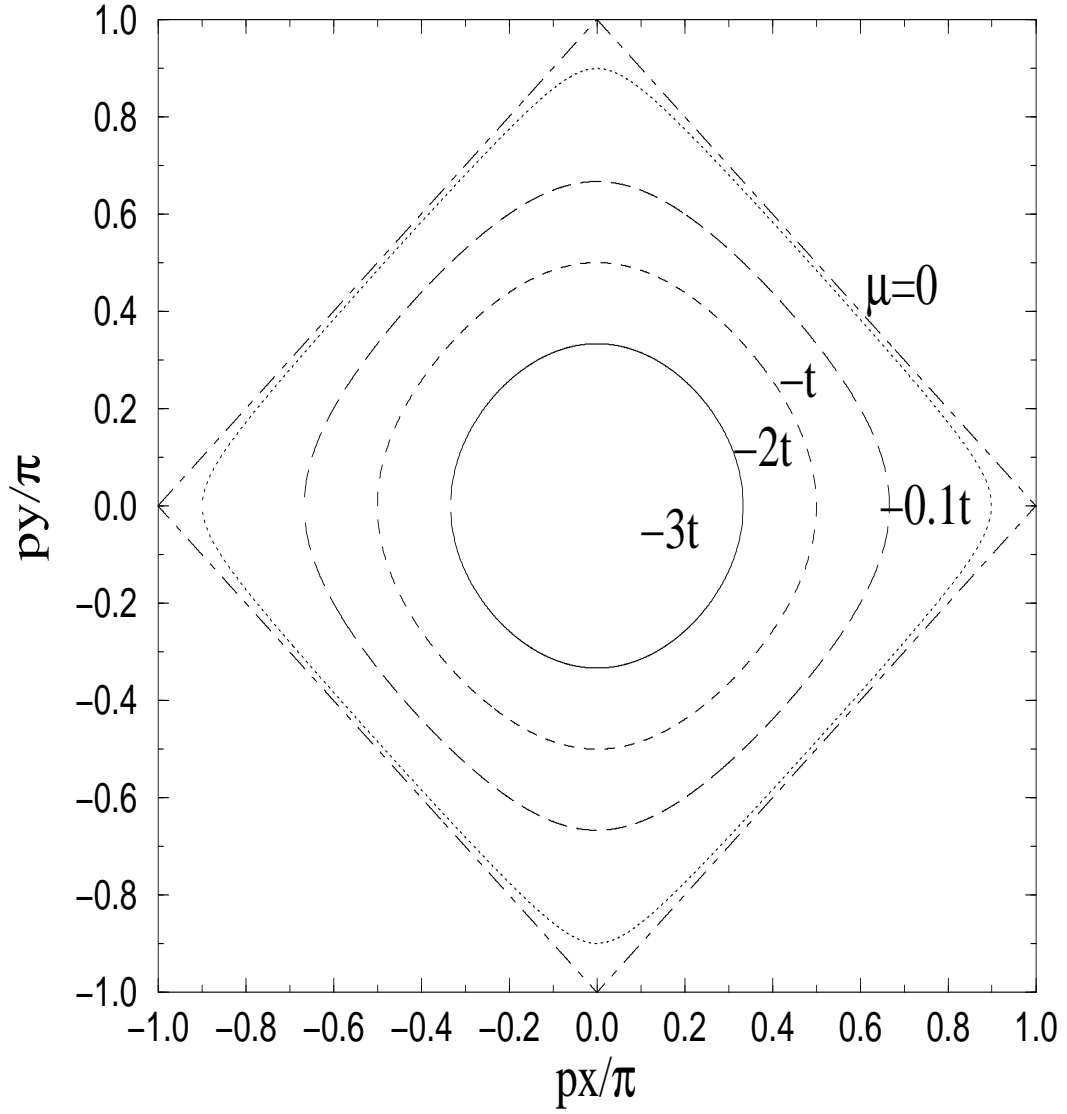


FIG. 1. The band structures for the tight-binding dispersion, $\xi_{\vec{p}} = -2t \cos p_x - 2t \cos p_y - \mu$ with different values of μ . As band is filled up, the parabolic Fermi surface is changes to a square surface. For $\mu = -0.1t$, there is a large region of flat Fermi surface.

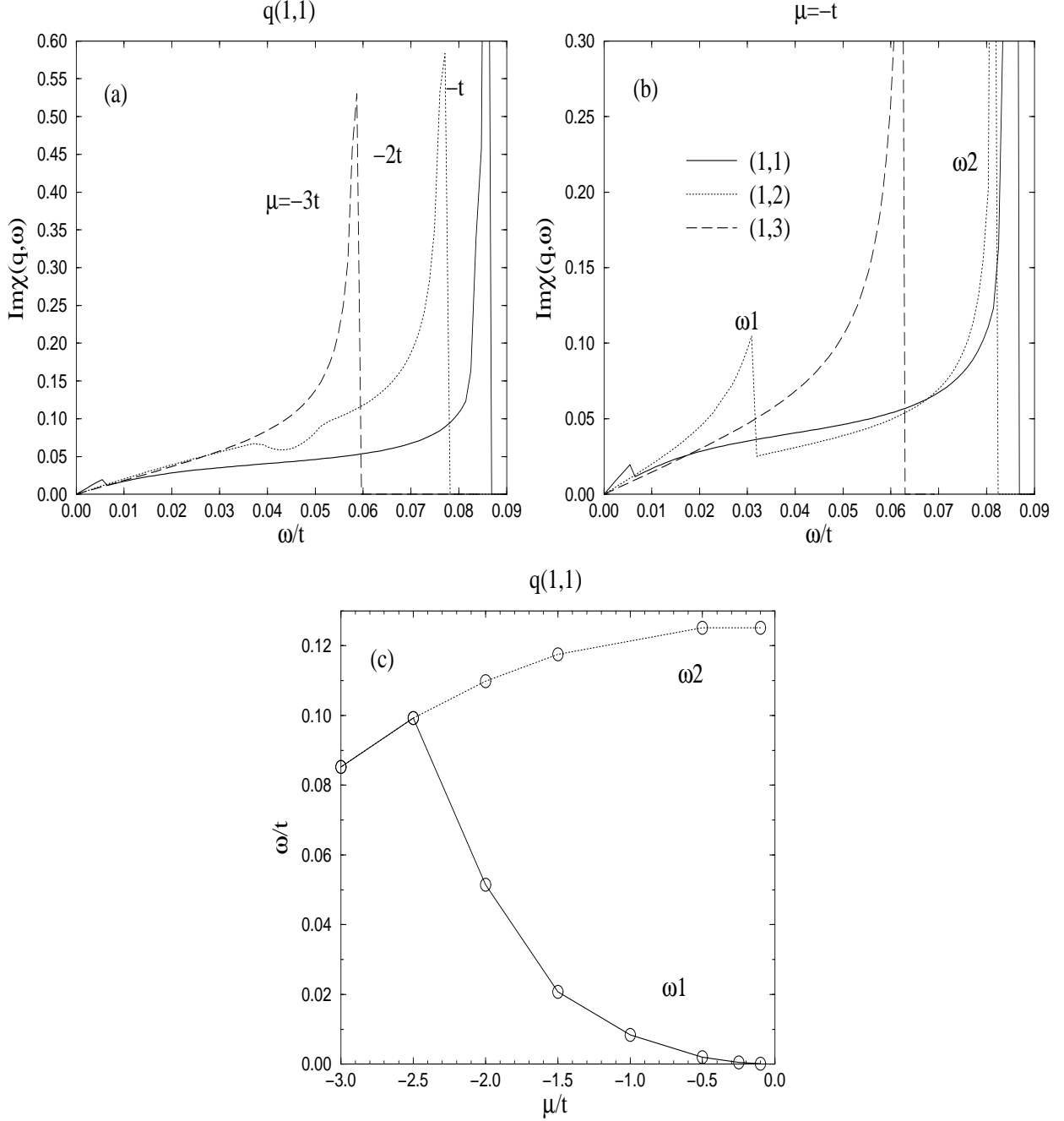


FIG. 2. The correlation functions as a function of μ and directions for $|\vec{q}| = 0.01\pi$. (a) χ'' as a function of μ . Two peaks are appeared in χ'' for the anisotropic band structure. (b) χ'' as a function of directions in \vec{q} . As \vec{q} points $(1, 0)\vec{q}$, ω_1 gets closed to ω_2 . (c) The locations of peaks in the correlation function, ω_1 and ω_2 . As $\mu \rightarrow 0$ the location of the first peak approaches to zero.

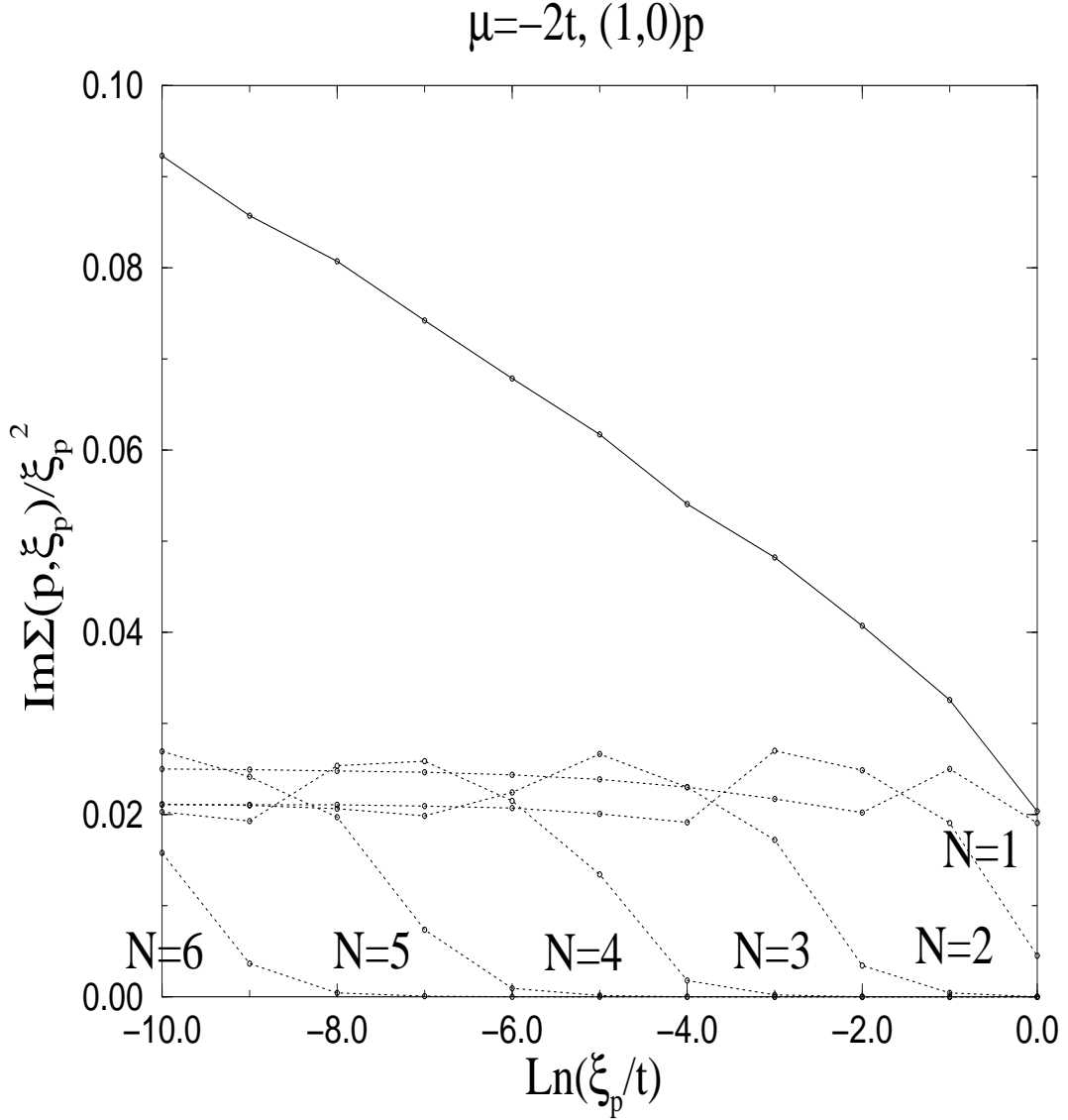


FIG. 3. The momentum contributions to the self-energy in second order calculations with $q = 10^{-N}\pi$. Each momentum is responsible for the log-behavior to the corresponding energies.

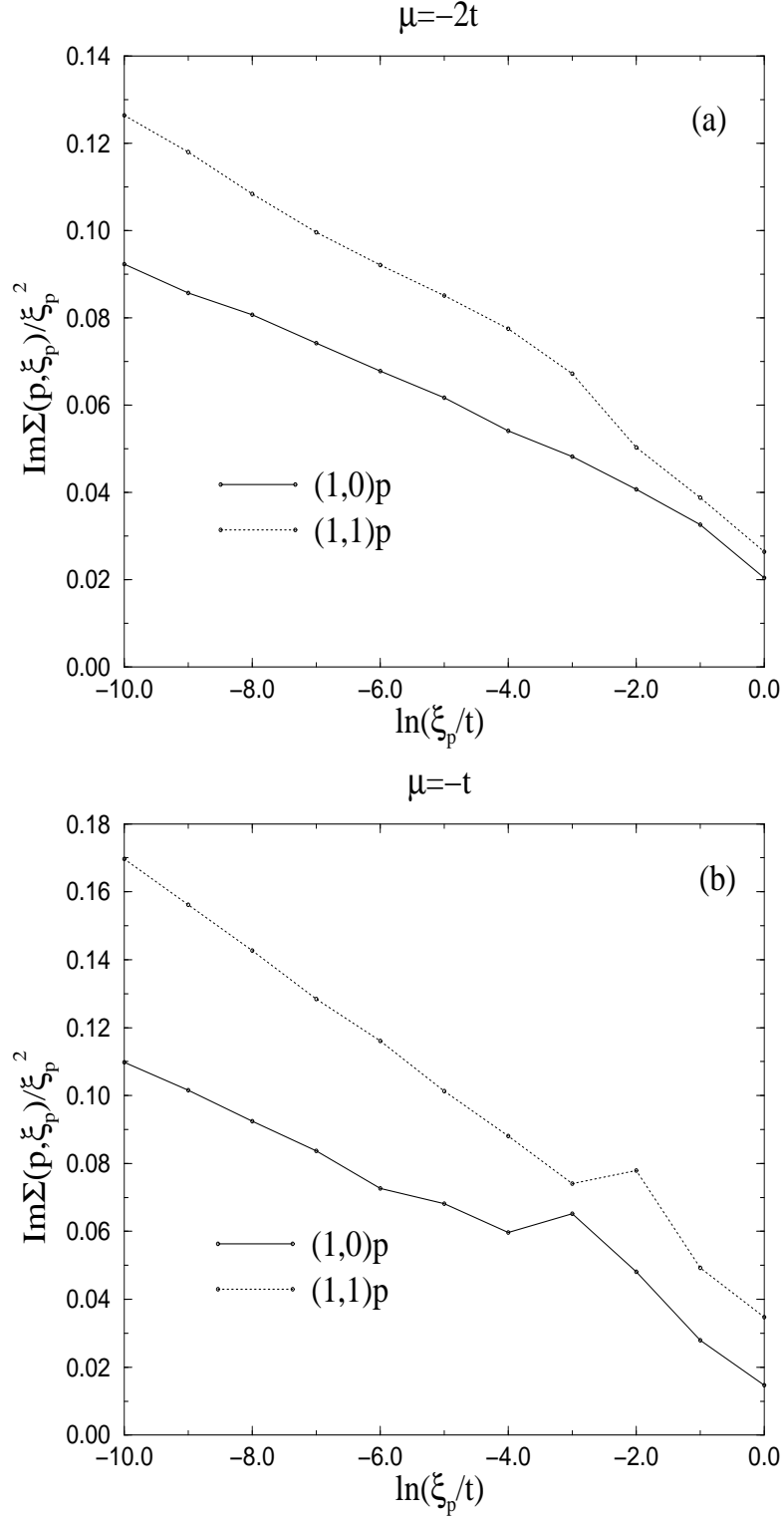


FIG. 4. The imaginary part of self-energies in second order calculations for $(1,0)p$ and $(1,1)p$ directions with (a) $\mu = -2t$ and (b) $\mu = -t$. Anisotropy increases in the magnitude of the self-energy as μ increases.

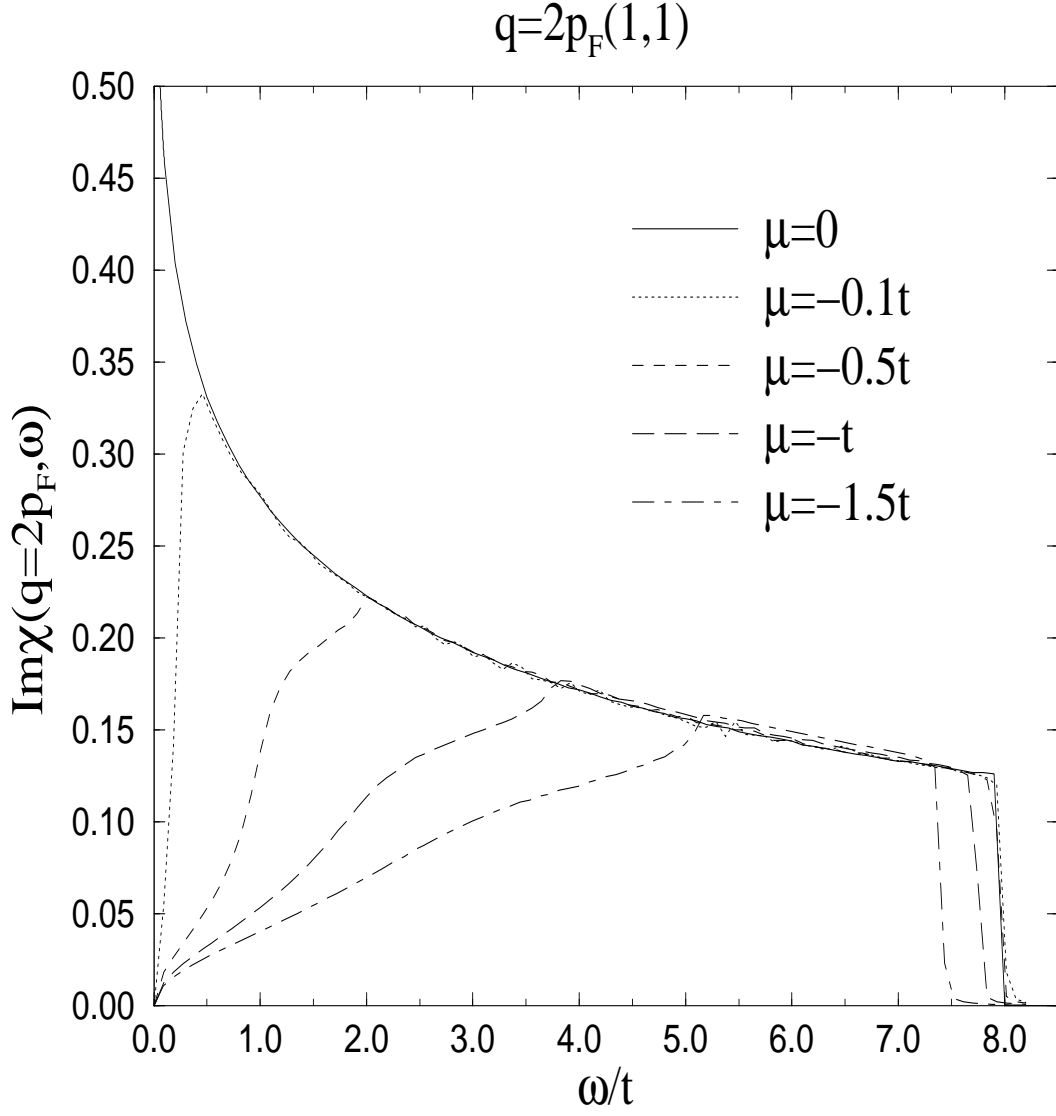


FIG. 5. The correlation functions for $q = 2p_F$ with different μ s. As $\mu \rightarrow 0$ logarithmic divergence is rapidly developed near $\mu \sim 0$.

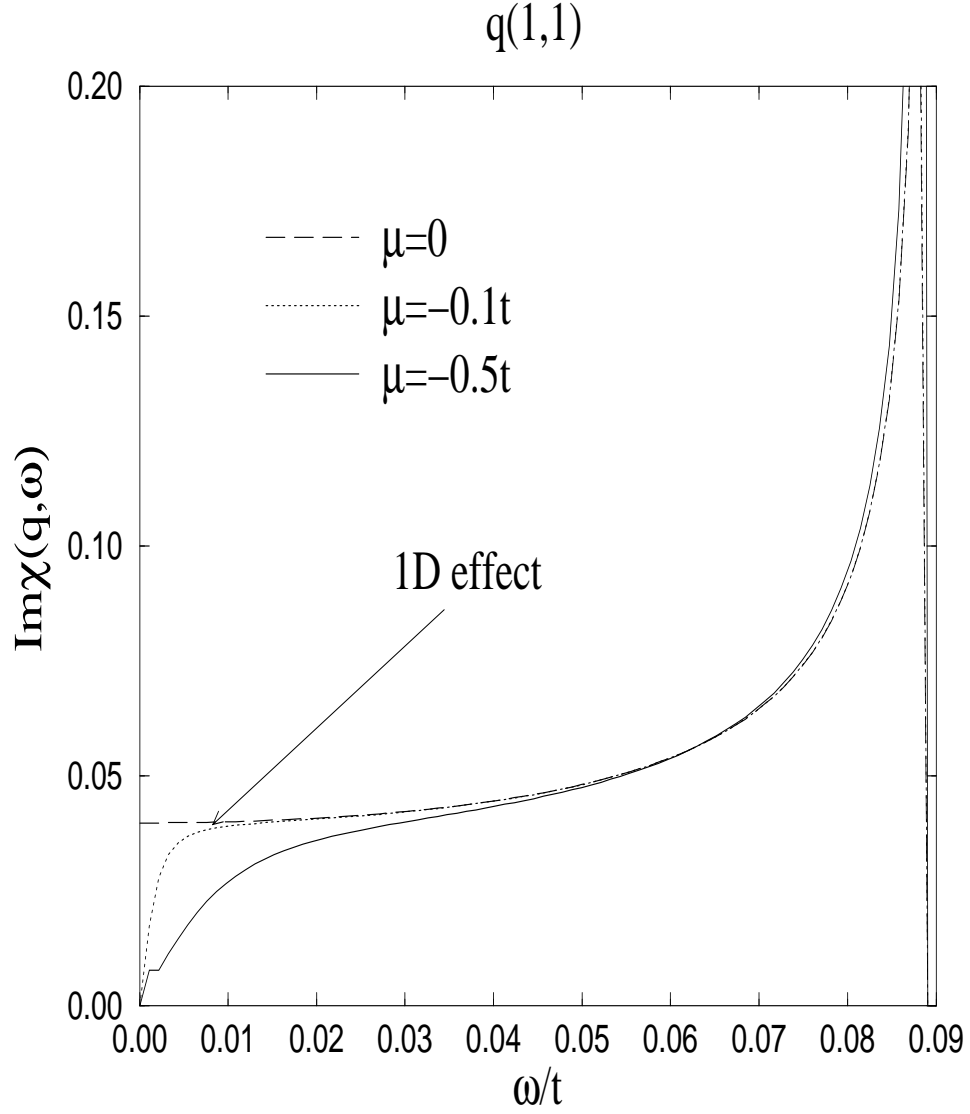


FIG. 6. The correlation functions for $q = 0.01\pi$ with different μ s. As $\mu \rightarrow 0$ ω independent behavior in low frequency is develops which is characteristic of 1D feature at long wavelengths and the system shows 1D effect.

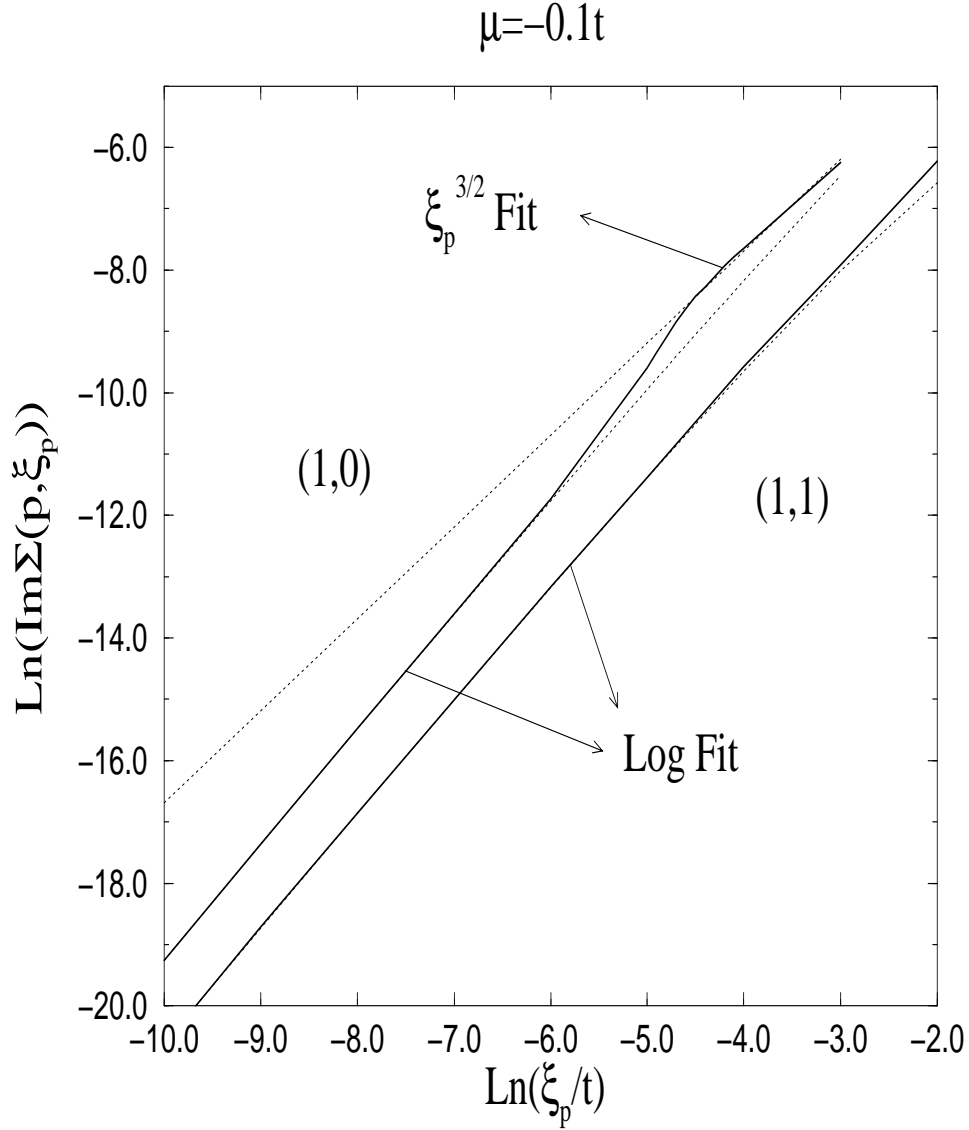


FIG. 7. The imaginary part of self-energy in second order calculations with $V = t$ shows $\xi^{3/2}$ behavior which is coming from frequency independent χ'' . This crossover from $\xi_p^2 \ln \xi_p$ to $\xi_p^{3/2}$ appears in (1,0) p direction. The dotted lines are fitted lines.

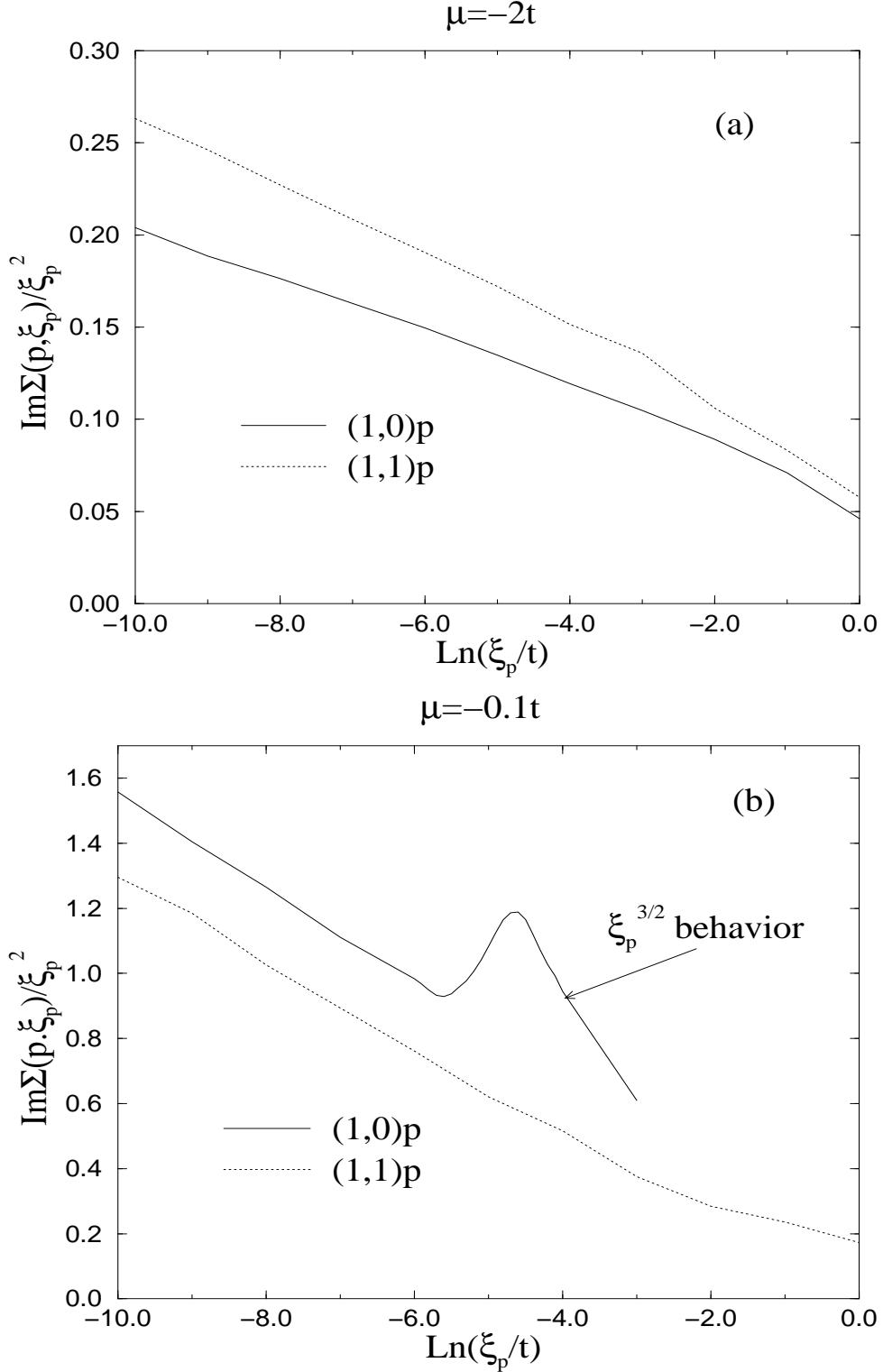


FIG. 8. The imaginary part of self-energies in RPA with $V = t$ for $(1,0)p$ and $(1,1)p$ directions with (a) $\mu = -2t$ and (b) $\mu = -0.1t$. For $\mu = -0.1t$ case, $\xi_p^{3/2}$ behavior for $(1,0)p$ direction appears as in 2nd order calculation. Both of the directions show the logarithmic behavior.

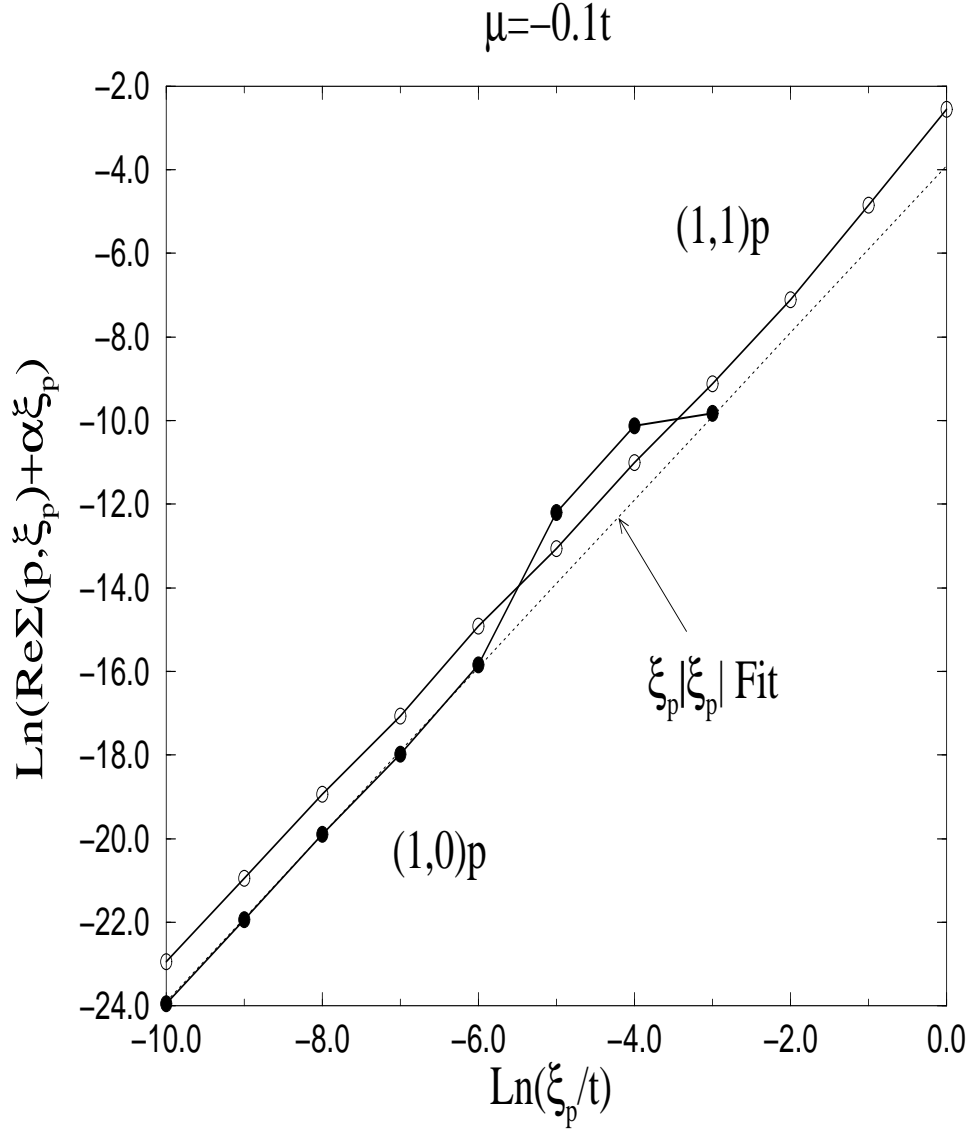


FIG. 9. The real part of self-energy calculated in RPA with $V = t$ shows $\xi|\xi_{\vec{p}}|$ behavior correction to $\alpha\xi_{\vec{p}}$ term. The slope 2 indicates the power of the fit. The deviation from the $\xi_{\vec{p}}|\xi_{\vec{p}}|$ behavior comes from the long wavelength quasi 1D frequency dependence of $\chi(\vec{q}, \omega)$.

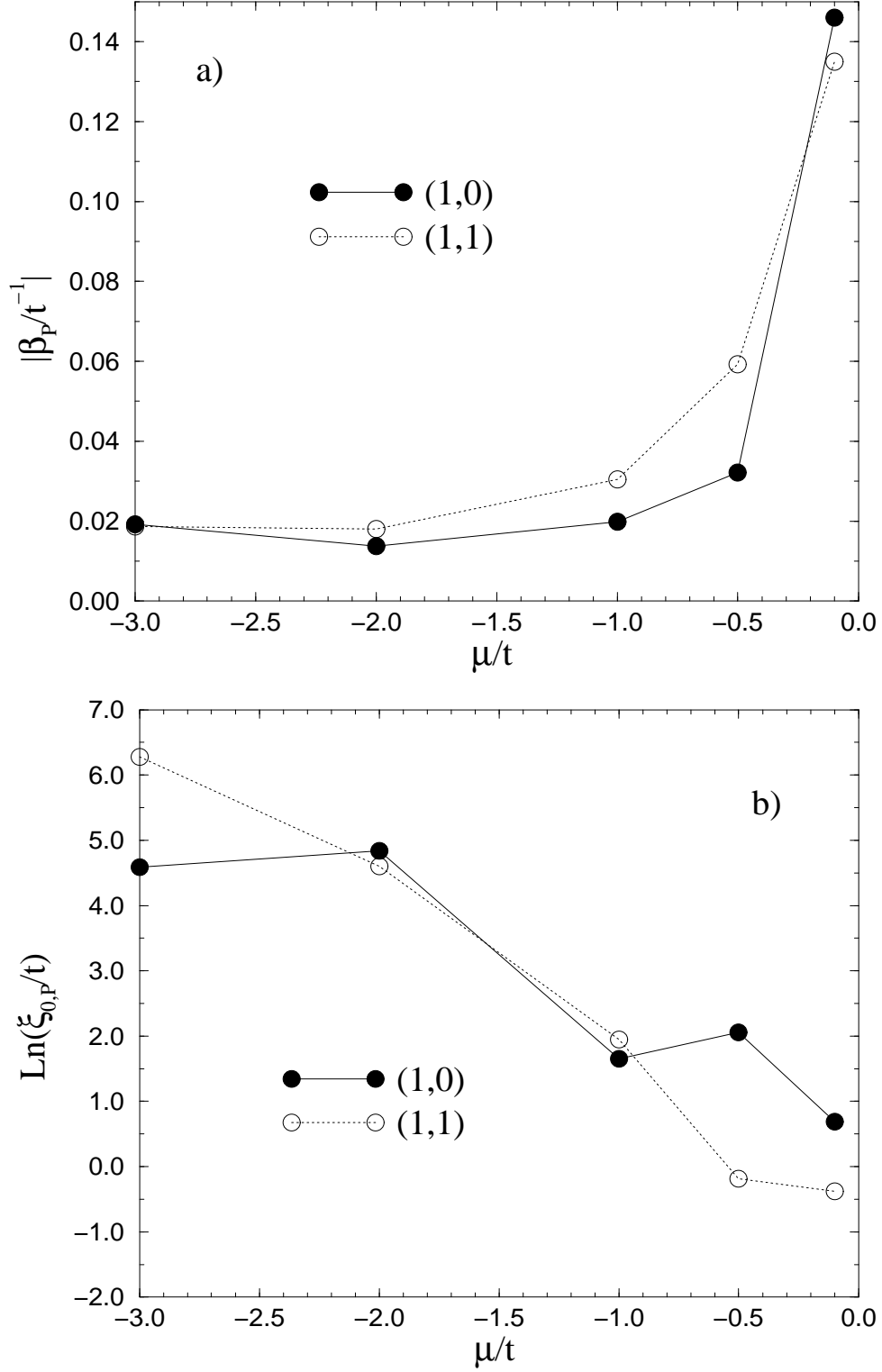


FIG. 10. The slopes, $\beta_{\vec{p}}$, (b) and the cut-off energies, $\xi_{0,\vec{p}}$ (a) in RPA as a function of μ from the form, $\Sigma''(\vec{p}, \xi_{\vec{p}}) = -\beta_{\vec{p}} \xi_{\vec{p}}^2 \ln \frac{\xi_{\vec{p}}}{\xi_{0,\vec{p}}}$.

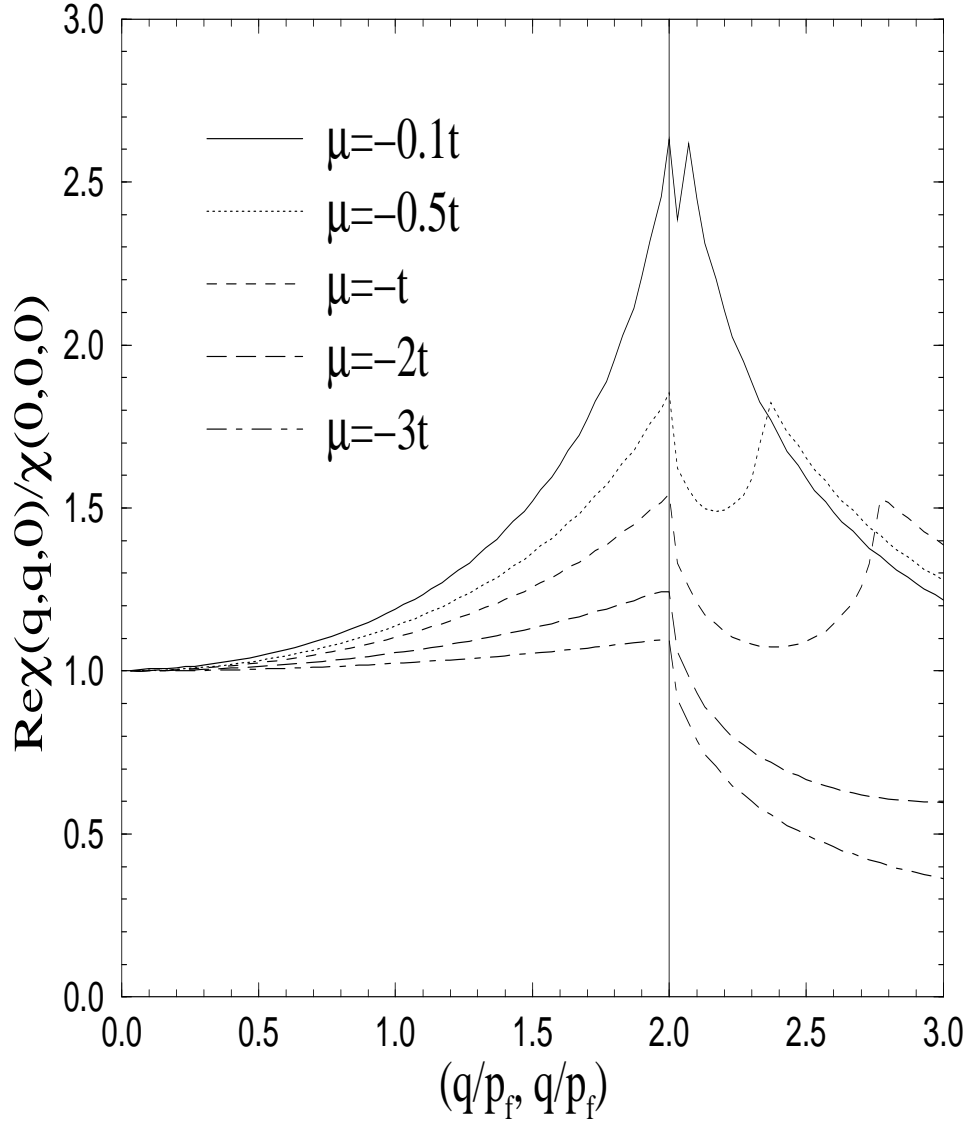


FIG. 11. The real part of the correlation function in static limit. The system changes 2D to 1D as $\mu \rightarrow 0$. A divergence grows at $q = 2p_f$ as $\mu \rightarrow 0$ in $(1, 1)q$ direction.

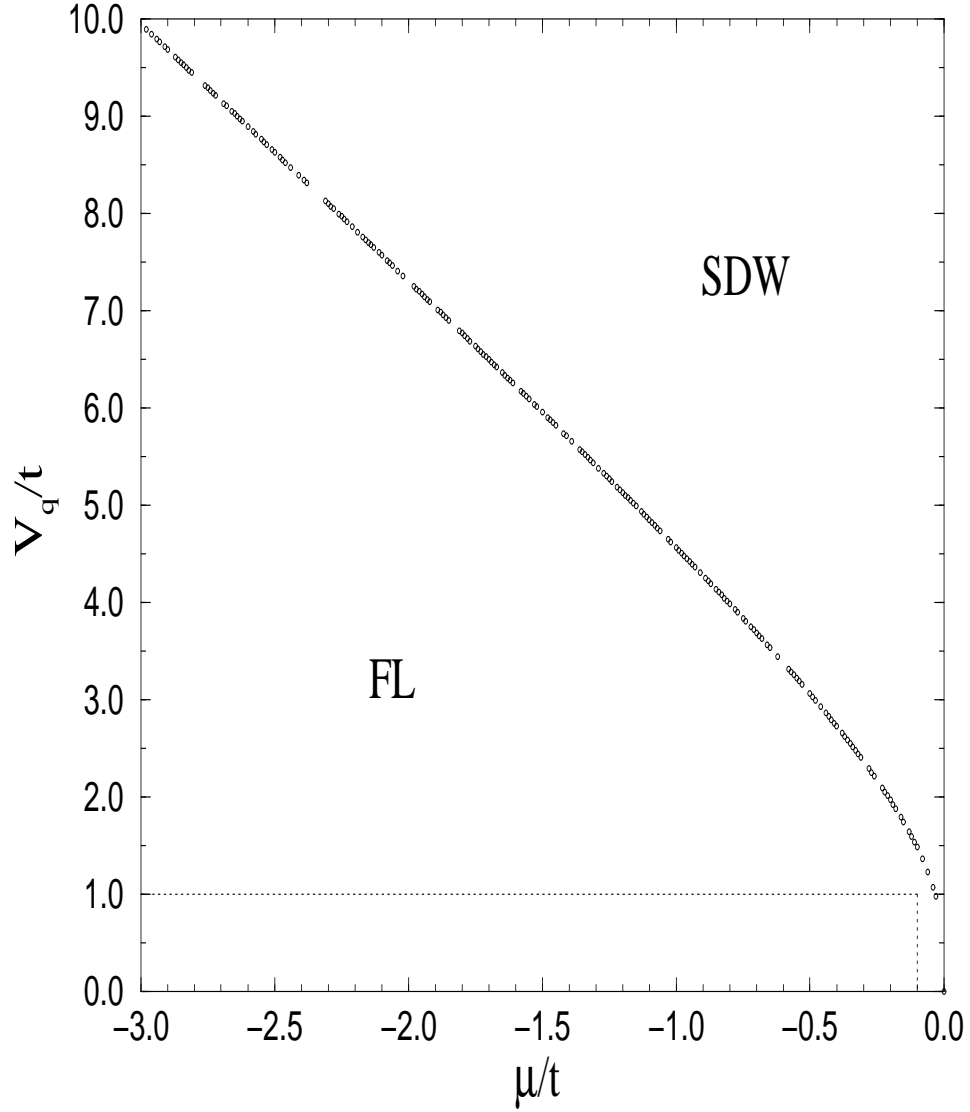


FIG. 12. The phase diagram of the system from $1 - V_q \chi'(2p_f, 2p_f, 0) = 0$. For any strength of interaction at $\mu = 0$ the quasi particle picture breaks down due to the divergence. With $V_q = t$, there is no SDW instability for $\mu < -0.1t$.

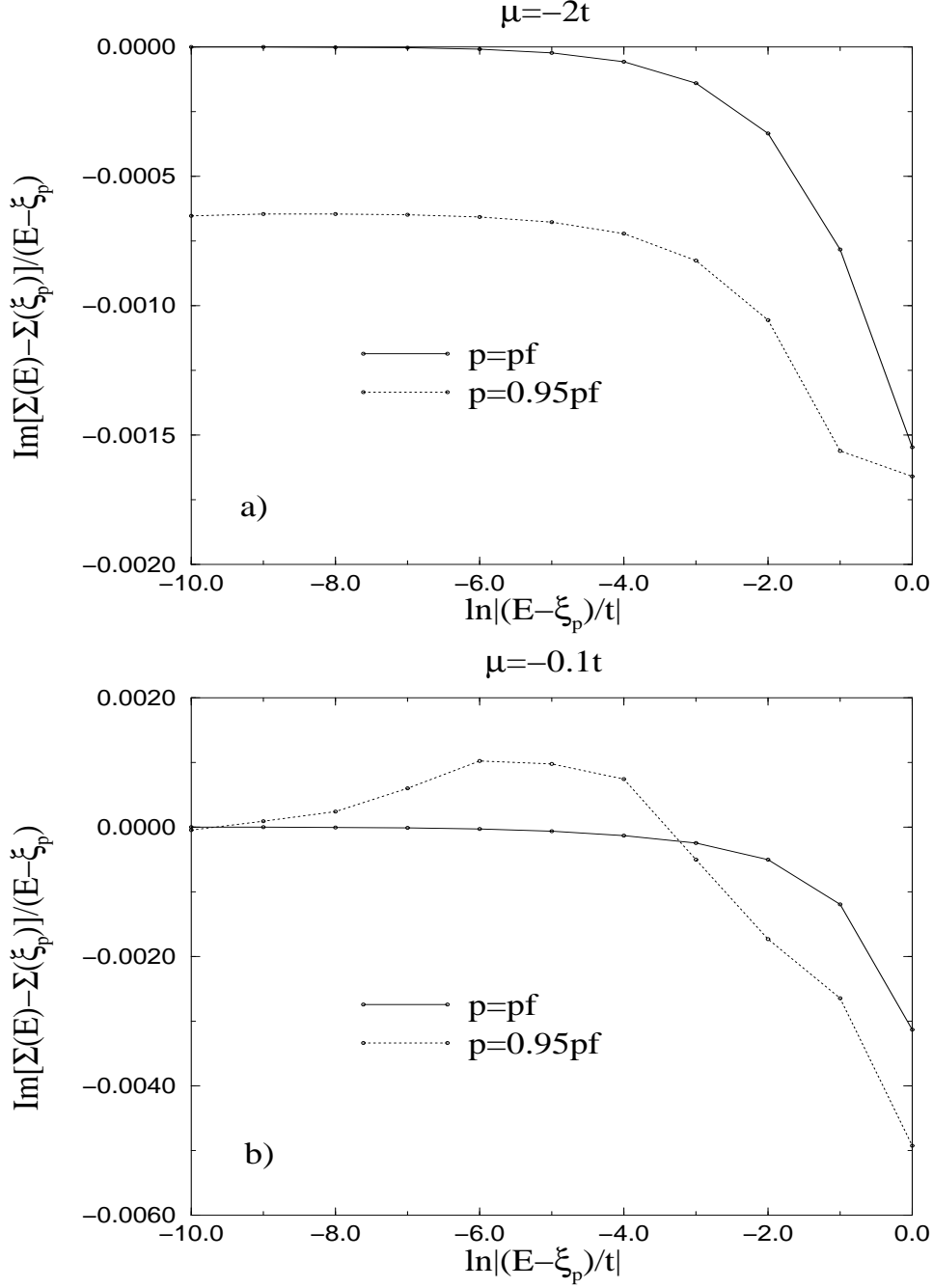


FIG. 13. The imaginary part of the off-shell self-energy for $E < 0$ and $p < p_f$ in second order calculations. $E \rightarrow \xi_{\vec{p}}$ limit $\Sigma''(\vec{p}, E)$ has constant energy term, $\xi_{\vec{p}}^2 \ln \xi_{\vec{p}}$, for $\mu = -2t$ in $\ln|E - \xi_{\vec{p}}|$ scale in the case of $p \neq p_f$. There is a significant deviations in $\Sigma''(\vec{p}, E)$ for $\mu = -0.1t$ in the case of $p \neq p_f$.

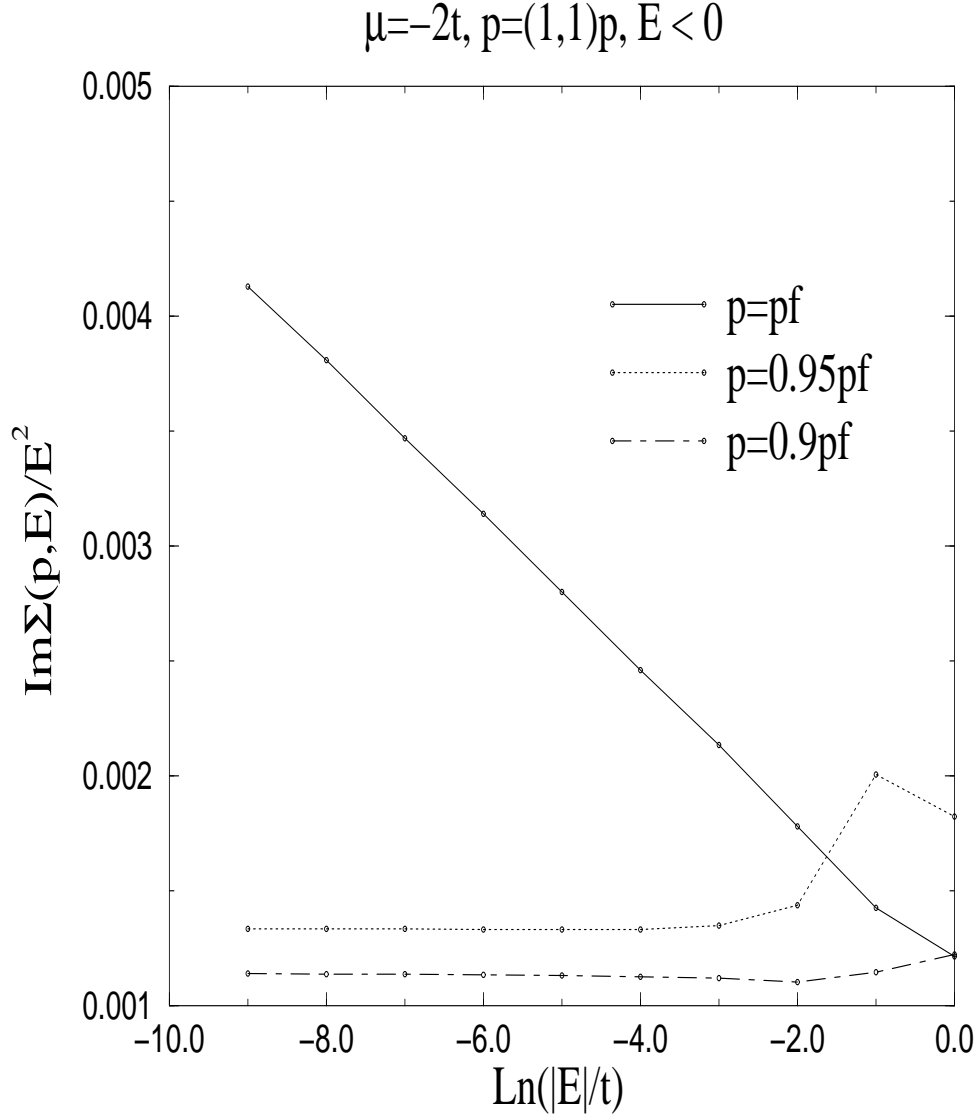


FIG. 14. The graph shows that the off-shell self energy follows $E^2 \ln E$ only when $p = p_f$ even for $\mu = -2t$ which is close to parabolic band structure.

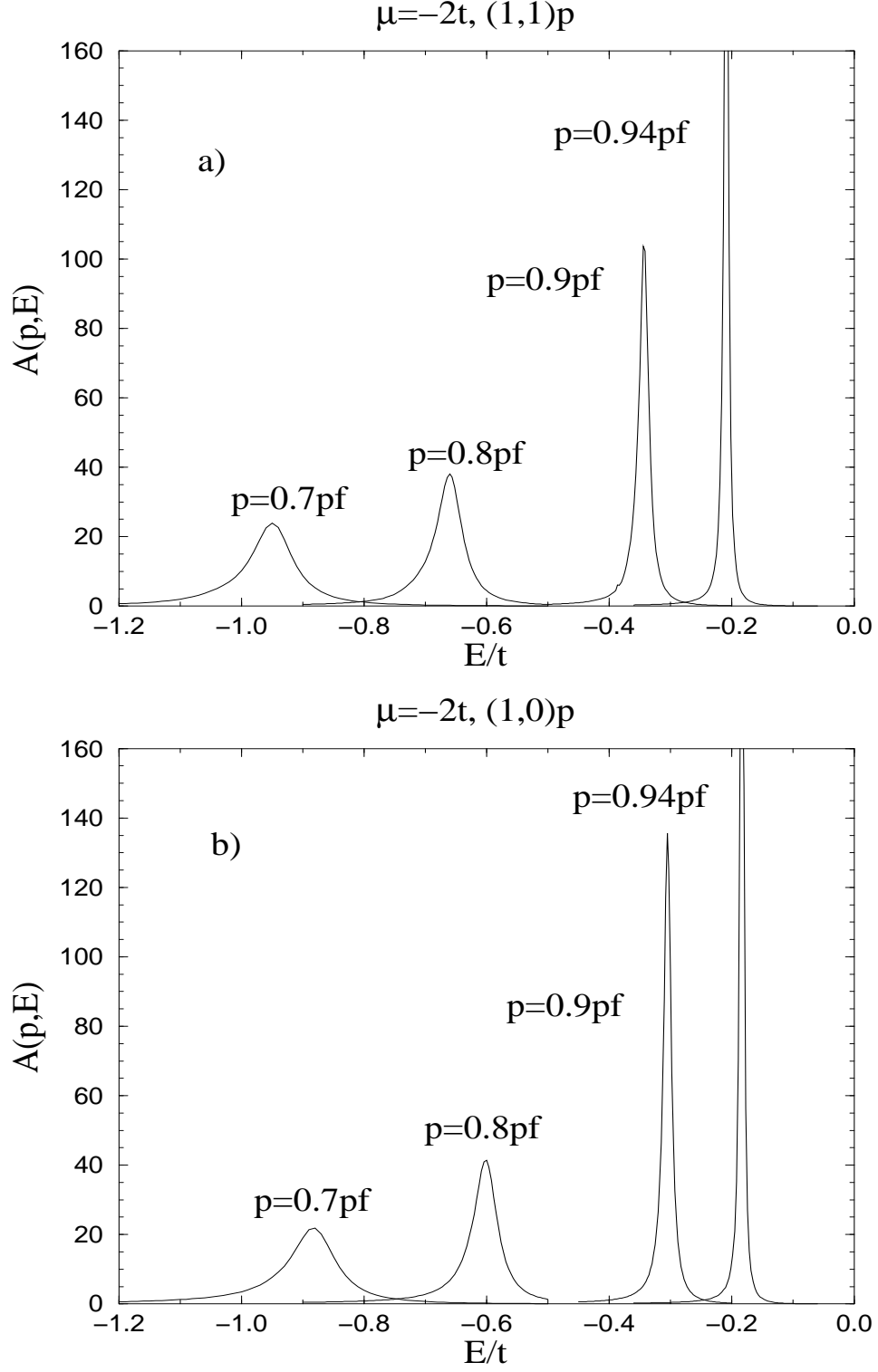


FIG. 15. The spectral functions in repeated scattering calculations for $\mu = -2t$ in $(1,1)\vec{p}$ (a) and $(1,0)\vec{p}$ (b) directions. The quasi-particle peakes are well defined as $p \rightarrow p_f$. Asymmetry in the resonance peak appears when $p \sim p_f$.

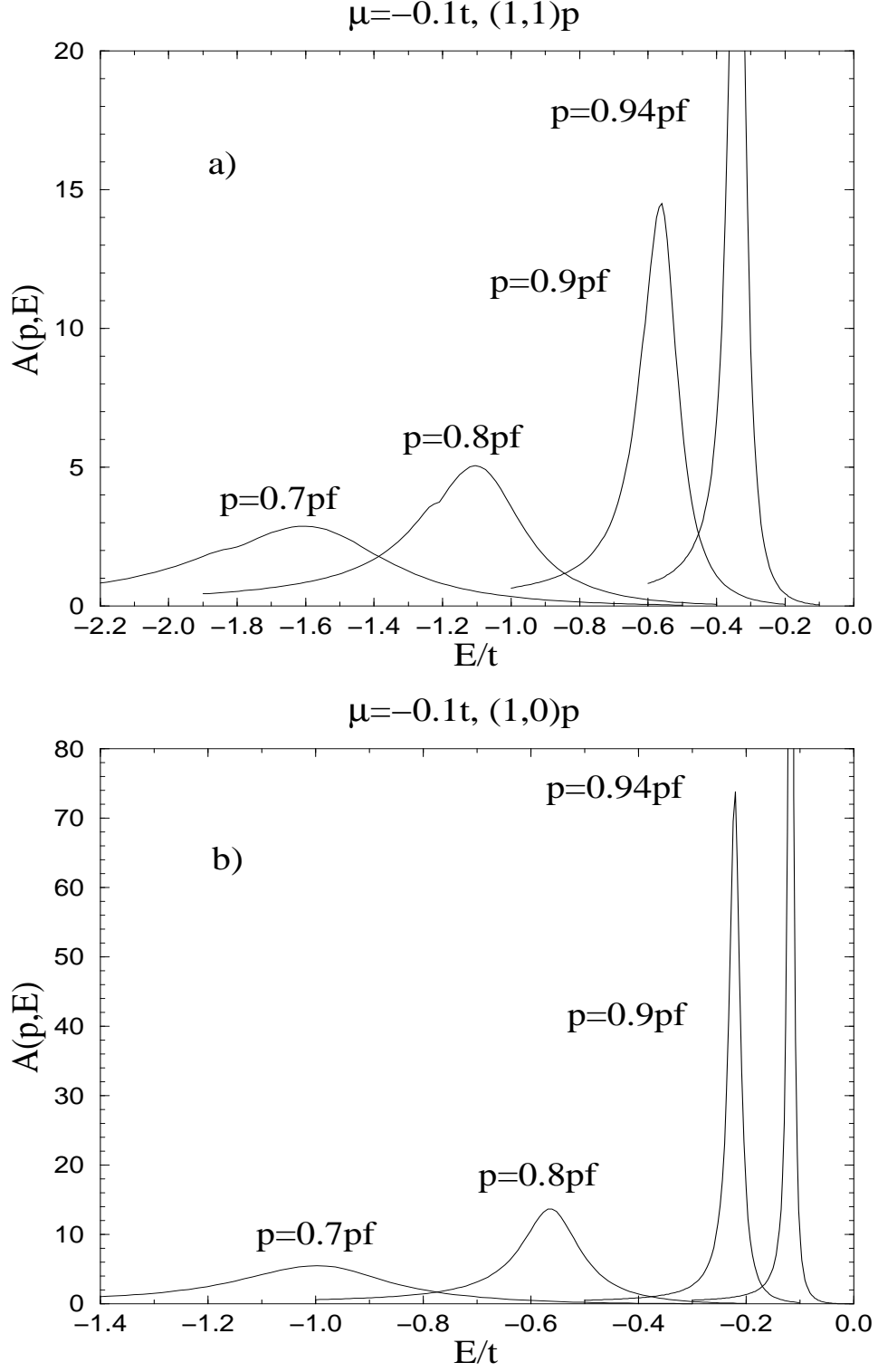


FIG. 16. The spectral functions in repeated scattering calculations for $\mu = -0.1t$ in $(1,1)\vec{p}$ (a) and $(1,0)\vec{p}$ (b) directions. The quasi-particle peakes are well defined as $p \rightarrow p_f$. Asymmetry in the resonance peak appears for $(1,1)\vec{p}$ in deep inside of Fermi surface.

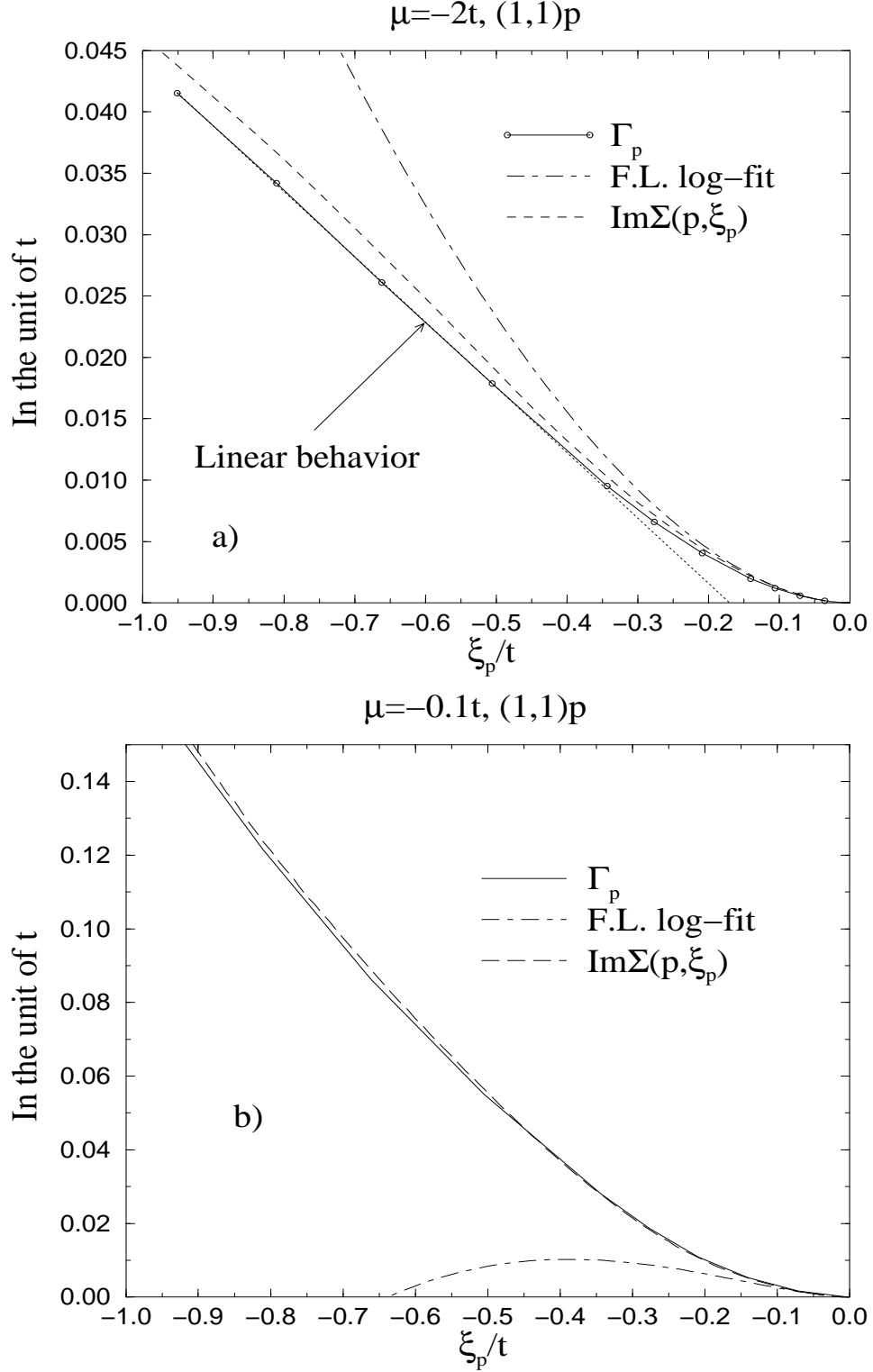


FIG. 17. The comparison between $\Gamma_{\vec{p}}$ and on-shell self-energy for $\mu = -2t$ (a) and $\mu = -0.1t$ (b). The FL behavior, $\xi_{\vec{p}}^2 \ln \xi_{\vec{p}}$, is restricted to low energies.